AD-A154 111 SENSITIVITY OF PLANETARY WAVES TO INITIAL CONDITIONS AND FORCING(U) NAVAL POSTGRADUATE SCHOOL MONTEREY CA M D MCATEE DEC 84 1/1

UNCLASSIFIED F/G 20/14 NL

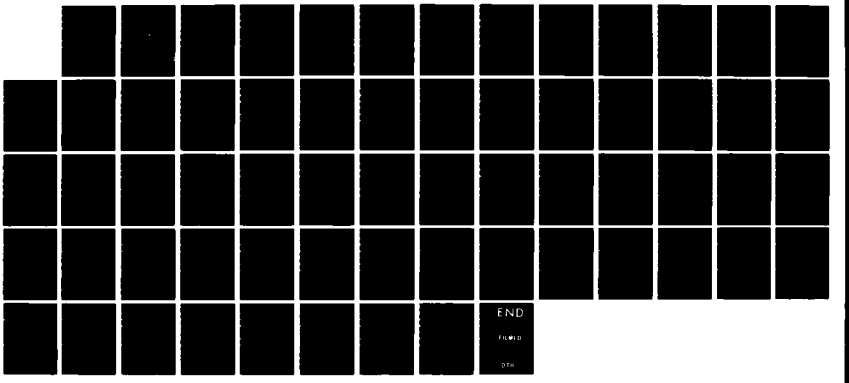

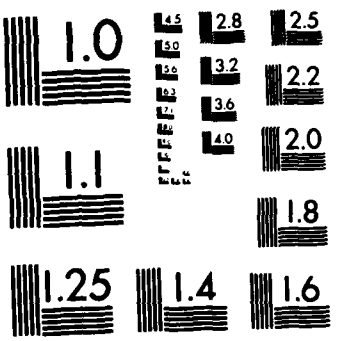

NAVAL POSTGRADUATE SCHOOL
Monterey, California

THESIS

SENSITIVITY OF PLANETARY WAVES
TO
INITIAL CONDITIONS AND FORCING

by

Michael D. McAtee

December 1984

Thesis Advisor: R. T. Williams

Approved for Public release; distribution unlimited.

SECURITY CLASSIFICATION OF THIS PAGE (When Data Entered)

REPORT DOCUMENTATION PAGE		READ INSTRUCTIONS BEFORE COMPLETING FORM
1. REPORT NUMBER	2. GOVT ACCESSION NO. A154 111	3. RECIPIENT'S CATALOG NUMBER
4. TITLE (and Subtitle) Sensitivity of Planetary Waves to Initial Conditions and Forcing		5. TYPE OF REPORT & PERIOD COVERED Master's Thesis: December 1984
		6. PERFORMING ORG. REPORT NUMBER
7. AUTHOR(s) Michael D. McAtee		8. CONTRACT OR GRANT NUMBER(s)
9. PERFORMING ORGANIZATION NAME AND ADDRESS Naval Postgraduate School Monterey, California 93943		10. PROGRAM ELEMENT, PROJECT, TASK AREA & WORK UNIT NUMBERS
11. CONTROLLING OFFICE NAME AND ADDRESS Naval Postgraduate School Monterey, California 93943		12. REPORT DATE December 1984
		13. NUMBER OF PAGES 61
14. MONITORING AGENCY NAME & ADDRESS(if different from Controlling Office)		15. SECURITY CLASS. (of this report) Unclassified
		15a. DECLASSIFICATION/DOWNGRADING SCHEDULE

16. DISTRIBUTION STATEMENT (of this Report)
Approved for public release; distribution unlimited.

17. DISTRIBUTION STATEMENT (of the abstract entered in Block 20, if different from Report)

18. SUPPLEMENTARY NOTES

19. KEY WORDS (Continue on reverse side if necessary and identify by block number)
Planetary Waves,
Spectral Model,
Harmonic Dial,
Normal Modes.

20. ABSTRACT (Continue on reverse side if necessary and identify by block number)

The sensitivity of planetary waves to various initial conditions and thermal forcing is examined using a linear global primitive equation spectral model.

Initial conditions are obtained by switching on a analytic heat source and then integrating the model equations out to 30 days. An averaging procedure is used to eliminate any transient modes which remained after integration so that the initial conditions represent steady state

DD FORM 1 JAN 73 1473 EDITION OF 1 NOV 65 IS OBSOLETE
S/N 0102-LF-014-6601

SECURITY CLASSIFICATION OF THIS PAGE (When Data Entered)

solutions. Additional integrations are performed in which 'errors' are introduced into the forcing and initial conditions.

Results of the study are examined using polar phase vs amplitude plots (harmonic dials) of various spherical harmonics. Results indicate that planetary waves are not sensitive to errors in the forcing or initial conditions. However, this lack of sensitivity is most likely due to the simplified initial conditions used in the model rather than to the inherent sensitivity of planetary waves.

Approved for public release; distribution is unlimited.

Sensitivity of Planetary Waves to Initial Conditions and Forcing

by

Michael D. McAtee
Captain, United States Air Force
B. A., University of California at Berkeley, 1978

Submitted in partial fulfillment of the
requirements for the degree of

MASTER OF SCIENCE IN METEOROLOGY

from the

NAVAL POSTGRADUATE SCHOOL
December 1984

Author: Michael D. McAtee
Michael D. McAtee

Approved by: R. T. Williams
R. T. Williams, Thesis Advisor

Mary Alice Rennick, Second Reader

R L Elsberry (Acting)
Robert J. Renard, Chairman,
Department of Meteorology

John N. Dyer
John N. Dyer,
Dean of Science and Engineering

ABSTRACT

The sensitivity of planetary waves to various initial conditions and thermal forcing is examined using a linear global primitive equation spectral model.

Initial conditions are obtained by switching on a analytic heat source and then integrating the model equations out to 30 days. An averaging procedure is used to eliminate any transient modes which remained after integration so that the initial conditions represent steady state solutions. Additional integrations are performed in which 'errors' are introduced into the forcing and initial conditions.

Results of the study are examined using polar phase vs amplitude plots (harmonic dials) of various spherical harmonics. Results indicate that planetary waves are not sensitive to errors in the forcing or initial conditions. However, this lack of sensitivity is most likely due to the simplified initial conditions used in the model rather than to the inherent sensitivity of planetary waves.

Ed. Keywords include: xx 1473

TABLE OF CONTENTS

LIST OF TABLES

LIST OF FIGURES

I. INTRODUCTION

Atmospheric predictability studies (Lorenz, 1969) indicate each scale of motion has a limit to it's predictability. Small scale motions are theoretically predictable to an hour, synoptic scales to a few days and planetary scales to a few weeks. However a number of studies, Lambert and Merilees (1978), Baumhefner and Downey (1978), and Morse (1983), have shown that synoptic scale motions, rather than planetary scale motions, are the most accurately forecast. Fig. 1.1 is taken from Daley et al (1981). It gives the 500mb geopotential forecast error from the 6-level National Center for Atmospheric Research global circulation model as a function of wavenumber. The error for each wavenumber has been normalized by the natural atmospheric variance for that wavenumber. Note that as previously stated the synoptic scales(wavenumbers 4-8) are in fact the most accurately forecast. This result does not seem to be dependent on the type of model used. Baumhefner and Downey examined a number of different models and found similar results. The error in forecasting planetary scale waves might not seem to be that important given that the error in the synoptic scales is smaller and that these are the scales of motion which produce most of the day to day weather changes. The importance of an accurate planetary scale comes to light when one starts to consider medium to long range forecasts (up to 10 days). Since the planetary waves often act to steer the smaller synoptic scale disturbances an improved planetary scale forecast would presumably lead to an improved forecast on the synoptic scale. In addition, the planetary waves contain a major portion of the eddy kinetic energy in the atmosphere and again a better long wave forecast would lead to a better synoptic scale forecast.

There are at least two possible reasons why planetary waves are not forecast as well as theory suggests. One is

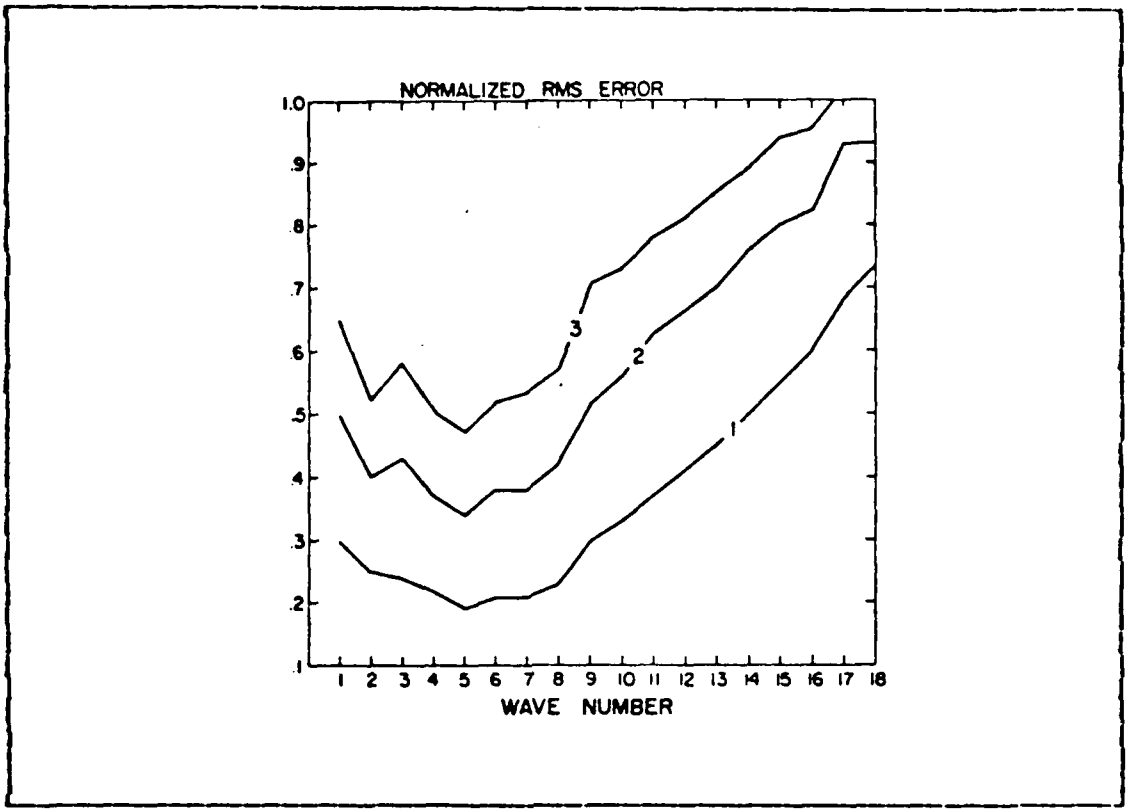

Figure 1.1 Forecast Errors for 1, 2 and 3 Days of Integration.

that the model dynamics for planetary waves are inadequate. Given that planetary waves are quasi-stationary in nature and are forced in part by differential heating and orography it would seem reasonable to suspect that inadequacies exist in the dynamics of the model's forcing. Another possibility is that current initialization procedures are not adequate for planetary scales.

It is the purpose of this study to examine the nature of planetary waves and to determine the sensitivity of

planetary waves to initial conditions and forcing. Chapter two of this thesis describes the model used in this study. The third chapter outlines the nature of the experiment. In the fourth chapter the results of the experiment are presented and in the final section these results are discussed and some conclusions are drawn.

II. MODEL DESCRIPTION

The model used in this study is a baroclinic spectral transform model which was developed by Rosmond (1977). Similar formulations have been carried out by Hoskins and Simmons (1975) and by Bourke (1974). The model is configured to include friction and/or diabatic heating. The specifics of how friction and diabatic heating are included in the model will be discussed in the next section. The basic equations of the model, in sigma coordinates, are as follows:

$$\frac{\partial \zeta}{\partial t} = -\vec{\nabla}\cdot(\zeta+f)\vec{V}-\vec{k}\cdot\vec{\nabla}\times(RT\vec{\nabla}q+\dot{\sigma}\frac{\partial \vec{V}}{\partial \sigma})+\vec{k}\cdot\vec{\nabla}\times\vec{F} \qquad (2.1)$$

$$\frac{\partial D}{\partial t} = \vec{k}\cdot\vec{\nabla}\times(\zeta+f)\vec{V}-\vec{\nabla}\cdot(RT\vec{\nabla}q+\dot{\sigma}\frac{\partial \vec{V}}{\partial \sigma})-\vec{\nabla}^2(\phi+\frac{\vec{V}^2}{2})+\vec{\nabla}\cdot F \qquad (2.2)$$

$$\frac{\partial q}{\partial t} = -D-\vec{V}\cdot\vec{\nabla}q-\frac{\partial \dot{\sigma}}{\partial \sigma} \qquad (2.3)$$

$$\frac{\partial \theta}{\partial t} = -\vec{V}\cdot\vec{\nabla}\theta+\dot{\sigma}\frac{\partial \theta}{\partial \sigma}+\frac{Q}{PCp} \qquad (2.4)$$

$$\frac{\partial \phi}{\partial \sigma} = -\frac{RT}{\sigma} \qquad (2.5)$$

where:

ζ - vorticity
D - divergence
T - temperature
θ - potential temperature
π - surface pressure
V - horizontal velocity vector
ϕ - geopotential height
R - gas constant
Cp - specific heat at constant pressure
f - Coriolis parameter

σ - vertical coordinate ($\sigma = P/\pi$)

$\dot{\sigma}$ - vertical velocity ($\dot{\sigma} = \frac{d\sigma}{dt}$)

q - ln

P - p

κ - R/Cp

F - frictional force

The continuity equation (Eq. 2.3) may be rewritten by integrating with respect to sigma and applying the boundary conditions $\dot{\sigma}(0)=\dot{\sigma}(1)=0$. Thus the integral of Eq. 2.3 maybe written as

$$\frac{\partial q}{\partial t} = -\overline{D}+\overline{G} \tag{2.6}$$

where $\overline{(\quad)} = \int_0^1 (\quad) d\sigma$ and $G= V \cdot \vec{\nabla} q$.

The vertical velocity, $\dot{\sigma}$, may be obtained diagnostically by substituting Eq. 2.6 into Eq. 2.3 and integrating in the vertical to obtain

$$\dot{\sigma} = (\overline{D}+\overline{G})\sigma - \int_0^\sigma (\overline{D}+\overline{G}) d\sigma \tag{2.7}$$

which uses $\dot{\sigma}(0)=0$

The first law of thermodynamics Eq. 2.4 can be written

$$\frac{\partial T}{\partial t} = -\vec{V}\cdot\vec{\nabla}T - \sigma^\kappa \dot{\sigma}\frac{\partial}{\partial\sigma}(T\sigma^{-\kappa}) + \kappa T(\frac{\partial q}{\partial t}+\vec{V}\cdot\vec{\nabla}q)+\frac{Q}{Cp} \tag{2.8}$$

In order to apply semi-implicit differencing it is necessary to divide temperature as follows:

$$T = T^*(\sigma)+T'(\sigma, \lambda, \Psi, t) \tag{2.9}$$

where T* represents an appropriately averaged temperature.

The basic equations can be conveniently written in spherical coordinates by defining the following operator:

$$\alpha(a,b) \equiv \frac{1}{1-x^2}\frac{\partial a}{\partial \lambda}+\frac{\partial b}{\partial x} \tag{2.10}$$

Using Eqs. 2.9 and 2.10 the basic equations can be written as follows:

$$\frac{\partial \zeta}{\partial t} = -\alpha(A,B) \tag{2.11}$$

$$\frac{\partial D}{\partial t} = -\alpha(A,B)-\vec{\nabla}^2(E+\phi+RT^*q) \tag{2.12}$$

$$\frac{\partial T}{\partial t} = -\alpha(UT',VT')+DT'-\sigma^{\kappa}\dot{\sigma}\frac{\partial}{\partial \sigma}(T\sigma^{-\kappa})+\kappa T(G-\bar{G}-\bar{D}) \tag{2.13}$$

$$\frac{\partial q}{\partial t} = -(\bar{D}+\bar{G}) \tag{2.14}$$

$$\sigma\frac{\partial \phi}{\partial \sigma} = -RT \tag{2.15}$$

where

$$A = (\zeta+f)U+\dot{\sigma}\frac{\partial V}{\partial \sigma}+\left(\frac{RT'}{r^2}\right)(1-x^2)\frac{\partial q}{\partial \lambda}-\frac{\sqrt{1-x^2}}{r}F_{\psi}$$

$$B = (\zeta+f)V-\dot{\sigma}\frac{\partial U}{\partial \sigma}-\left(\frac{RT'}{r^2}\right)\frac{\partial q}{\partial \lambda}+\frac{\sqrt{1-x^2}}{r}F_{\lambda}$$

$$G = \frac{U}{1-x^2}\frac{\partial q}{\partial \lambda}+V\frac{\partial q}{\partial x}$$

$$E = (U^2+V^2)/2(1-x^2)$$

$$U = u(\cos\Psi)/r$$

$$V = v(\cos\Psi)/r$$

$$x = \sin\Psi$$

Ψ = latitude

λ = longitude

Eqs. 2.10 - 2.15 are the basic equations used in the model. These equations are represented spectrally in the horizontal and finite differenced in the vertical.

A. VERTICAL STRUCTURE

The vertical structure of the model follows the development given by Arakawa and Suarez (1983). The variables are staggered in σ so that ζ, D, U, V and T are carried at the mid-point of each layer where $\sigma = \hat{\sigma}_k$ and $\dot{\sigma}$ is carried at the top and bottom of each layer where $\sigma = \sigma_k$. The vertical structure is illustrated in Fig. 2.1. The finite difference form of Eqs. 2.10 - 2.15 are

$$\frac{\partial \zeta}{\partial t} = -\alpha_k(A,B) \tag{2.16}$$

$$\frac{\partial D_k}{\partial t} = \alpha_k(B,-A)-\vec{\nabla}^2(\phi_k+RT^*q+E_k) \tag{2.17}$$

$$\frac{\partial q}{\partial t} = -(\overline{G}+\overline{D}) \tag{2.18}$$

$$\frac{\partial T_k}{\partial t} = -\alpha_k(UT',VT')T'D_k + T^*_k(G_k-\overline{G}-\overline{D})- \tag{2.19}$$

$$\frac{1}{\Delta\sigma_k}\{\dot{\sigma}_{k+1}B_k(\frac{P_k}{P_{k+1}}T_{k+1}-T_k)+ A_k(T_k-\frac{P_k}{P_{k-1}}T_{k-1}\}+Q/Cp$$

$$\phi_k-\phi_{k+1} = Cp(P_{k+1}-P_k)(\frac{A_kT_k}{P_k}+\frac{B_kT_{k+1}}{P_{k+1}}) \tag{2.20}$$

$$\phi_{LM} = \phi_s+CpT^*_{LM}(\frac{P^\kappa}{P_{LM}}-1) \tag{2.21}$$

$$\dot{\sigma}_{k+1} = \sigma_{k+1}(G+D)-\sum_{j=1}^{k}(G_j+D_j)\Delta\sigma_j \tag{2.22}$$

where

$$\hat{P}_k = (\sigma_{k+1}\pi)^\kappa$$

$$P = (\frac{\pi^\kappa}{1+\kappa})(\sigma^{1+\kappa}_{k+1}\sigma^{1+\kappa}_k)/(\sigma_{k+1}-\sigma_k)$$

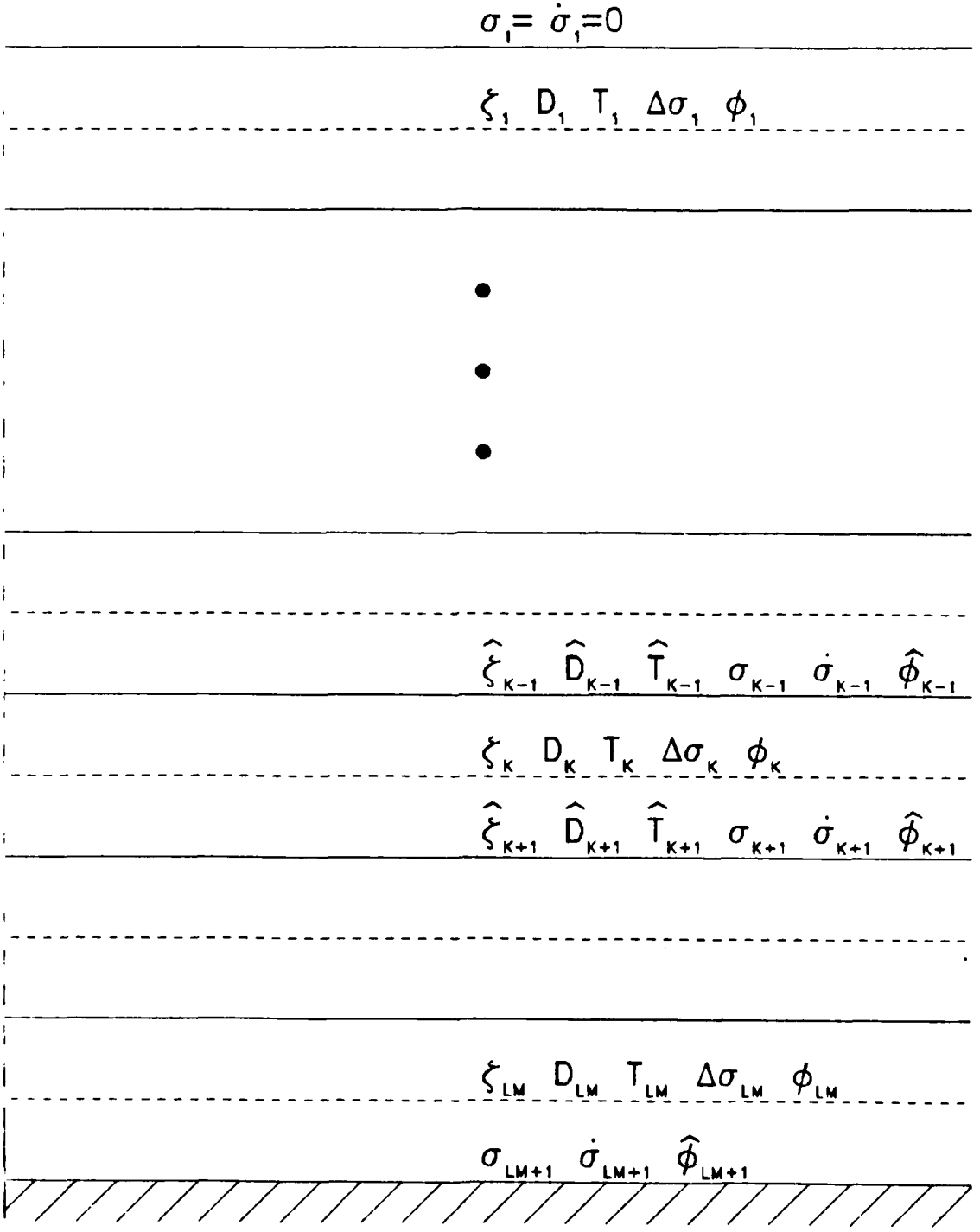

Figure 2.1 Vertical Structure.

$$A = (\zeta+f)U_k+\{\dot{\sigma}_{k+1}(V_{k+1}-V_k)+\dot{\sigma}_k(V_k-V_{k-1})\}/2\Delta\sigma_k$$

$$+\{RT'_k(1-x^2)/r^2\}\frac{\partial q}{\partial x} -(\sqrt{1-x^2}/r)F_\psi$$

$$B = (\zeta+f)V_k+\{\dot{\sigma}_{k+1}(U_{k+1}-U_k)+\dot{\sigma}_k(U_k-U_{k-1})\}/2\Delta\sigma_k$$

$$-(CpRT'_k/r)\frac{\partial q}{\partial x} +(\sqrt{1-x^2}/r)F_\lambda$$

$$G = \vec{V}_k\cdot\vec{\nabla}\pi/\pi$$

$$D = \vec{\nabla}\cdot\vec{V}_k$$

$$A_k = (\hat{P}_k-P_k)/(P_{k+1}-P_k)$$

$$B_k = (P_{k+1}-\hat{P}_k)/(P_{k+1}-Pk)=1-A_k$$

Eqs. 2.16 - 2.22 can be written in matrix form, such that the terms on the right hand sides contain all the terms which are to be evaluated explicitly and the left hand side contains those terms which are to be evaluated implicitly. Eq. 2.20 can be combined with an integrated finite difference form of Eq. 2.15 to obtain

$$\phi = \underline{\underline{C}}\ T+\phi_s \qquad (2.23)$$

where $\underline{\underline{C}}$ is a square matrix and the other quantities are column vectors. The finite difference form of the surface pressure tendency equation (Eq. 2.14) is

$$\frac{\partial q}{\partial t} = \Sigma(G_k+D_k)\Delta\sigma_k \qquad (2.24)$$

which can be written in matrix form as

$$\frac{\partial q}{\partial t} = -N^T(G+D) \qquad (2.25)$$

where N^T is the transpose of a constant column vector. Similarly Eq. 2.22 can be written

$$\sigma = Z(G+D) \tag{2.26}$$

The next to last term in Eq. 2.19 is

$$\dot{\sigma}_{k+1}B_k\left(\frac{P_k}{P_{k+1}}T_{k+1}-T_k\right)+\dot{\sigma}_k A_{k-1}\left(T_k-\frac{P_k}{P_{k-1}}T_{k-1}\right) \tag{2.27}$$

For the purpose of semi-implicit formulation, the temperature is separated according to Eq. 2.9. The mean part of that term can be written as

$$\dot{\sigma}_{k+1}B_k\left(\frac{P_k}{P_{k+1}}T^*_{k+1}-T^*_k\right)+\dot{\sigma}A_{k-1}\left(T^*_k-\frac{P_k}{P_{k-1}}T^*\right) = \underline{\underline{M}}(G+D) \tag{2.28}$$

Eqs. 2.17, 2.19, 2.23, and 2.25 may now be written:

$$\frac{\partial \vec{D}}{\partial t}+\vec{\nabla}^2(\vec{\phi}'+\underline{R}\vec{T}^*q)=\alpha(B,-A)-\vec{\nabla}^2 E = \vec{K}_D \tag{2.29}$$

$$\frac{\partial q}{\partial t}+\vec{N}^T\vec{D} = -\vec{N}^T\vec{G} \tag{2.30}$$

$$\frac{\partial \vec{T}}{\partial t}+\underline{\underline{Q}}\,\vec{D} = \vec{K}_T \tag{2.31}$$

$$\vec{\phi}' = \underline{\underline{C}}\,\vec{T} \tag{2.32}$$

where $\underline{\underline{Q}} = \underline{\underline{M}} + \kappa T^* N^T$ and $\phi = \phi - \phi_s$ and K_D and K_T represent terms which have not been explicitly separated out.

The semi-implicit time differencing is achieved by evaluating the terms on the left hand sides of Eqs. 2.29, 2.30 and 2.31 implicitly. The remaining terms and Eq. 32 are evaluated explicitly using leapfrog differencing. The difference equations can now be written

$$\vec{D}_{n+1}+\Delta t\vec{\nabla}^2(\underline{\underline{C}}\,\vec{T}_{n+1}+\underline{R}\vec{T}^*q_{n+1}) = \vec{D}_{n-1}-\Delta t\vec{\nabla}^2(\underline{\underline{C}}\,\vec{T}_{n-1}+\underline{\underline{P}}\vec{T}^*q_{n-1})+2\Delta t(\vec{K}_D)_n \tag{2.33}$$

$$\vec{T}_{n+1}+\Delta t\underline{\underline{Q}}\vec{D}_{n+1} = \vec{T}_{n-1}-\Delta t\underline{\underline{Q}}\vec{D}_{n-1}-2\Delta t(\vec{K}_T)_n \quad (2.34)$$

$$q_{n+1}+\Delta t\vec{N}^T\vec{D} = q_{n-1}-\Delta t\vec{N}^T\vec{D}_{n-1}-2\Delta t\vec{N}^T\vec{G}_n \quad (2.35)$$

Now the following equation for D can be found by substituting Eq. 2.34 and 2.35 into 2.33:

$$B_-\vec{D}_{n+1} = B_+\vec{D}_{n-1}+2\Delta t(\vec{K}_D)_n-2\Delta t\vec{\nabla}^2(\underline{\underline{C}}\vec{T}_{n-1}+\underline{\underline{R}}\vec{T}^*q_{n-1}+\underline{\underline{C}}(\vec{K}_T)_n \quad (2.36)$$
$$-\underline{\underline{R}}\vec{T}^*\vec{N}^T\vec{G}_n$$

where the matrix operator B is

$$B_\pm = \Delta t^2(\underline{\underline{C}}\ \underline{\underline{Q}}\pm\underline{\underline{R}}\vec{T}\vec{N}^T)\vec{\nabla}^2+\underline{\underline{I}} \quad (2.37)$$

B. SPECTRAL FORMULATION

The equations (2.10)-(2.15) are represented spectrally in the horizontal. The variables are represented as follows:

$$C(\lambda, x, \sigma, t) = \sum_{m=-J}^{J}\sum_{n=|m|}^{J} C_n^m(\sigma, t)P_n^m(x)e^{im\lambda} = \quad (2.38)$$
$$\sum_{m=-J}^{J}\sum_{n=|m|}^{J} C_n^m Y_n^m$$

where C is some variable and $(C_n^m)^* = (-1)^m C_n^{-m}$

m = zonal wavenumber

n = meridional index, and n-|m| gives the number of zeros between the poles $(-1 \le x \le 1)$ of the associated Legendre function

J = truncation limit (for this study triangular truncation was used with J=3)

λ = (l-1)/2 nondimensional zonal coordinate index $(1 \le l \le 16)$

Note that the separation is such that the coefficients C_n^m are functions of time and the vertical and the spherical harmonic Y_n^m are horizontal functions of space. The normalization and orthogonality properties of the Y_n^m allow the coefficients to be obtained as follows:

$$C_n^m = \langle C, Y_n^m \rangle \equiv \frac{1}{4\pi} \int_0^{2\pi} \int_{-1}^{+1} C Y_n^m dx d\lambda \qquad (2.39)$$

The non-linear terms are computed using the transform method following Haltiner and Williams (1980). The longitudinal direction is treated with a Fast Fourier Transform and the latitudinal direction uses Gaussian Quadrature. The number of latitudes, N and longitudes M satisfy.

$N \geq 3J/2 + 1$ $\qquad$ $M \geq 3J+1$

The number of points are chosen so that there will be no aliasing from the product terms. For this study N=4 and M=16. It was discovered just before this study was completed that number of Gaussian latitudes used to compute the latitudinal integrals was actually J+1 and not 3J/2 + 1. However, model integrations using J +1 latitudes are not qualitatively different than those using 3J/2 + 1 latitudes. Even the quantitative differences are small, and will occur mostly in the non-linear integrations. Since the cases examined in this study are carried out using a linear form of the model, one would not expect much error.

III. EXPERIMENT DESIGN

The intent of this study is to specify a known analytic heating function on a planetary scale and then integrate the equations until the model atmosphere reaches a steady or quasi-steady state. These steady state solutions will be altered and/or the heating will be changed. The equations will then be integrated again to determine the sensitivity of planetary waves to changes in the forcing and initial conditions

Heating is introduced into the model via the thermodynamic equation (2.4). Q is specified to be a Legendre function of the form:

$$Q(\lambda, x, \sigma) = \sum_{m=-J}^{J} \sum_{n=|m|}^{J} A_n^m(\sigma) P_n^m(x) e^{im\lambda} \qquad (3.1)$$

A_n^m is specified to have the vertical structure:

$$A_n^m = Ae^{\frac{1-\sigma}{.3}} \qquad (3.2)$$

Only one wave form is forced at a time and the other heating amplitudes are set to zero. The constant A is chosen to give a reasonable temperature response. In most cases a temperature response of a few degrees is used.

Before the heating is "turned on" the model atmosphere is specified to be in a state of solid rotation

$$\bar{U} = \quad \cos$$
$$\bar{V} = 0$$

such that $\bar{U}$ = 20 m/s(15.5 °/day) at the equator. The surface pressure field is chosen to balance the mean flow. The initial vertical temperature distribution is given by the standard atmosphere values consistent with the pressure

distribution given by solid rotation. A lapse rate of 6.5° per kilometer is specified to the top of the model atmosphere.

TABLE I
Waves Forced for Linear Cases

Case	Wave Forced	
	m	n
1	1	1
2	1	2
3	1	3
4	2	2
5	2	3
6	3	3

In all of the experiments the model is run in a linear mode. In this mode the amplitudes of all zonal wavenumbers except those being forced are held constant. The model is run in a linear mode in these experiments to allow a more definitive interpretation of the results. Six linear cases are integrated, each case with a different forced wave form. For example in case 1 (see Table I) zonal wavenumber one (m=1), meridional index one (n=1) is forced. The results from these cases are fairly similar so only the longest wave case (case 1) is analyzed in detail.

Two classes of cases are examined using the steady state values. In the first, the magnitude of the heating function is changed and the model is integrated from the steady state values. In the second, the magnitude of the steady state values are changed and then used as initial conditions for further model integrations. In the these cases the heating function is the same as the one originally used to bring the model to a steady state.

IV. RESULTS

Due to the similarity of the six linear cases only cases 1, 5 and 6 will be discussed. These three cases represent the three zonal wavenumbers(1, 2 and 3) and the two basic meridional structures possible in the model. Cases 1 and 6 are symmetric in their meridional structure while case 5 is anti-symmetric. The primary tool used to analyze these cases was the harmonic dial. These diagrams are polar plots of phase and amplitude for a given spherical harmonic. This plot has the advantage that the quasi-stationary and transient nature of the waves are easily seen. Fig. 4.1 is a good example upon which the merits of the harmonic dial can be explained. In this figure the phase and amplitude for the temperature wave for case 1 are plotted every 12 h. The elapsed time since the start of the integration is indicated every 5 days. For an ideal case where there is a stationary and a transient component one would expect to see a circular pattern which is confined to a particular quadrant. This is because as the transient wave moves through the staticnary wave it will come in and out of phase with the stationary wave. The maximum amplitude occurs when the transient and stationary waves are completely in phase and the minimum amplitude occurs when the waves are 180° out of phase. A rough estimate of the phase speed of the transient wave can be obtained by observing the change in phase with time as plotted on the diagrams. The direction of propagation can be determined by observing the direction of the phase change on the dial. A counterclockwise change in phase indicates eastward propagation, a clockwise change indicates westward propagation. In Fig. 4.1 the phase speed of the temperature wave at $\sigma = .925$ can be easily estimated. The period of the

wave is 21.5 days, thus the phase speed in degrees per day is 360/21.5=16.74. The direction of propagation is east-

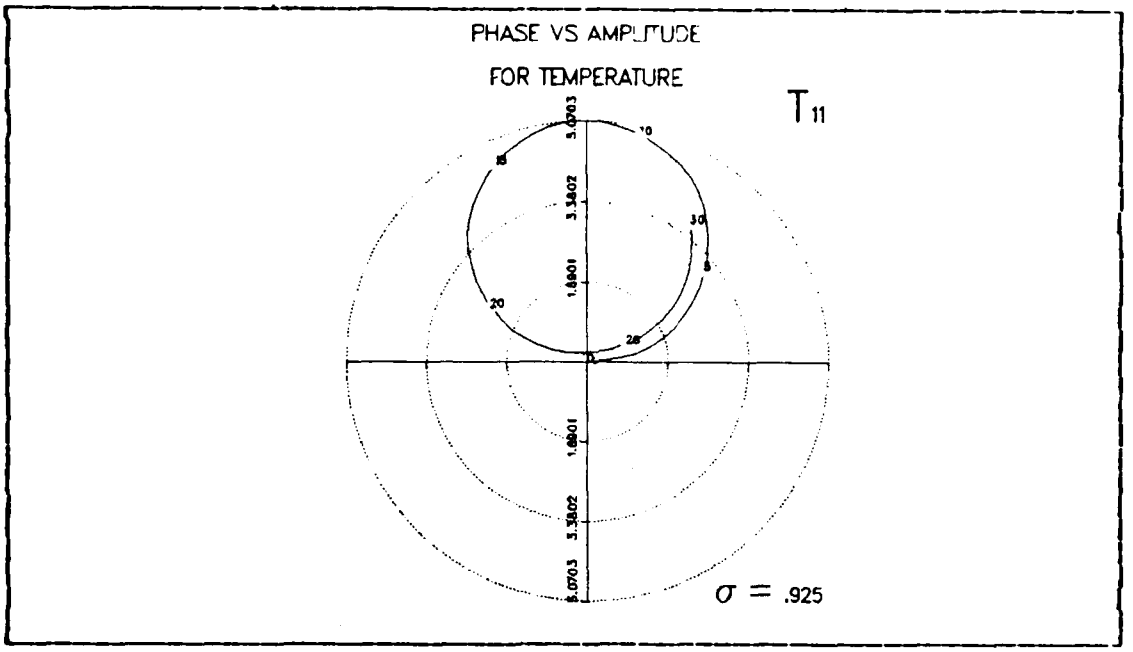

Figure 4.1 Harmonic Dial for Case 1 Temperature Component.

ward. Another important point to note here is that, given the uniformity of the change in phase, the phase speed of the transient component is constant. The harmonic dials for surface pressure, temperature and the zonal(U) and meridional(V) wind components for the lowest model level are shown in Figs. 4.2 - 4.7 . Only those components which have significant amplitude are shown in these figures. In all cases the pressure and winds waves show a much more irregular pattern than the temperature wave. These irregularities might be due to the presence of a number of transient modes components with periods much less than that indicated by the overall pattern. Table II gives the estimated period (in days) and phase speed (in °/days) for the temperature, surface pressure and the V and U wind component waves for

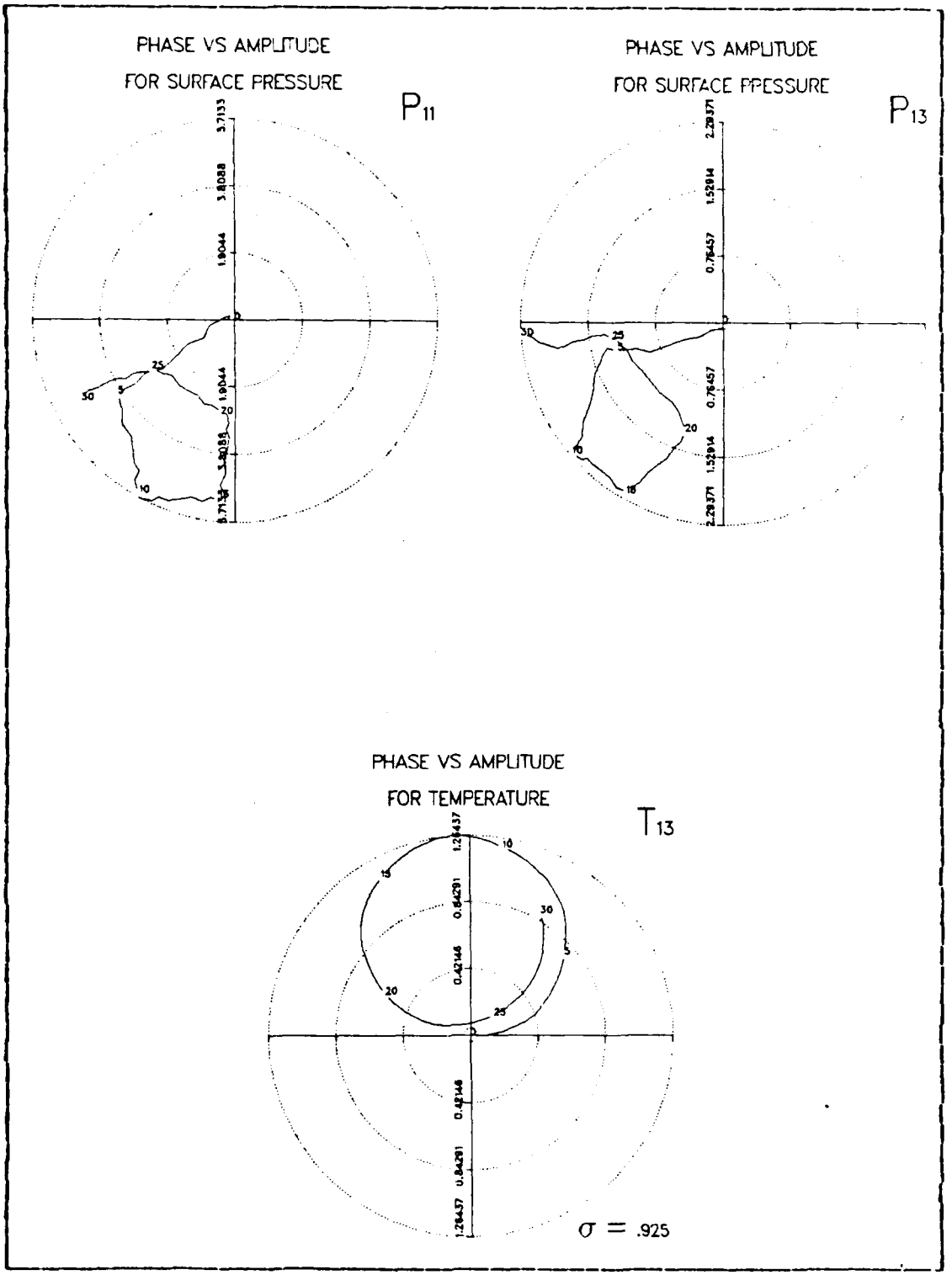

Figure 4.2 Harmonic Dials for Temperature and Surface Pressure for Case 1.

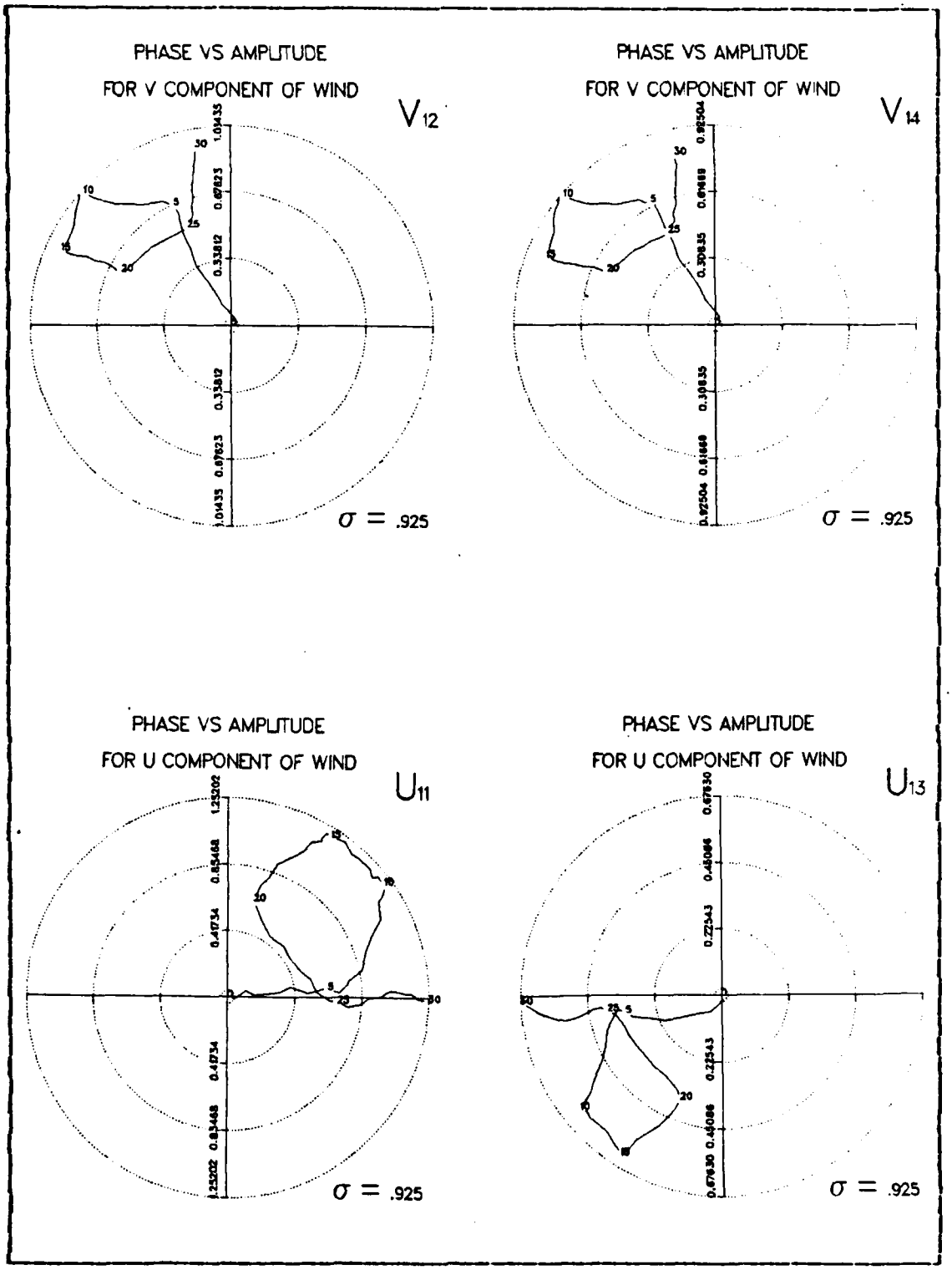

Figure 4.3 Harmonic Dials for Meridional(U) and Zonal(U) Wind Case 1.

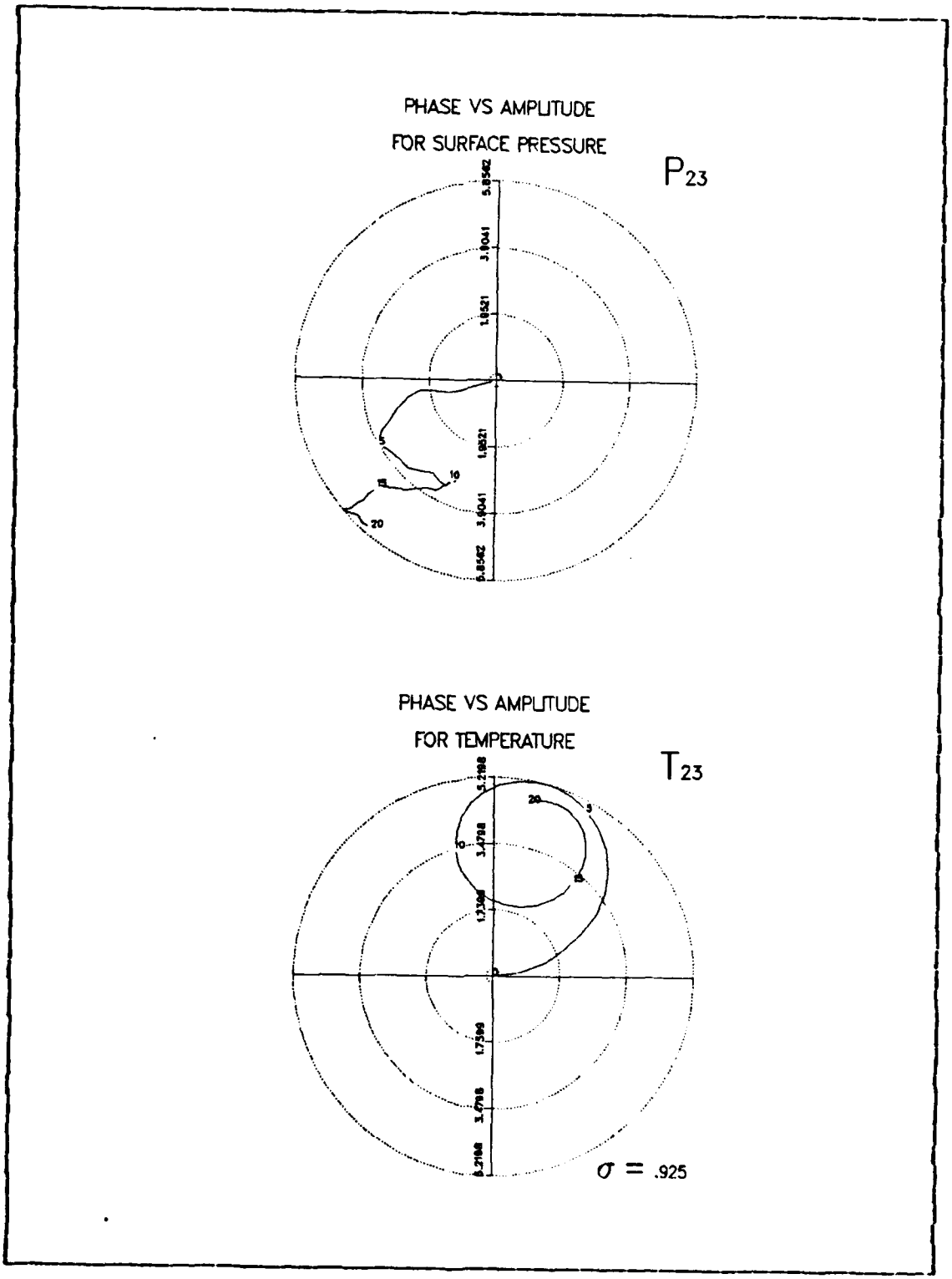

Figure 4.4 Harmonic Dials for Temperature and Surface Pressure for Case 5.

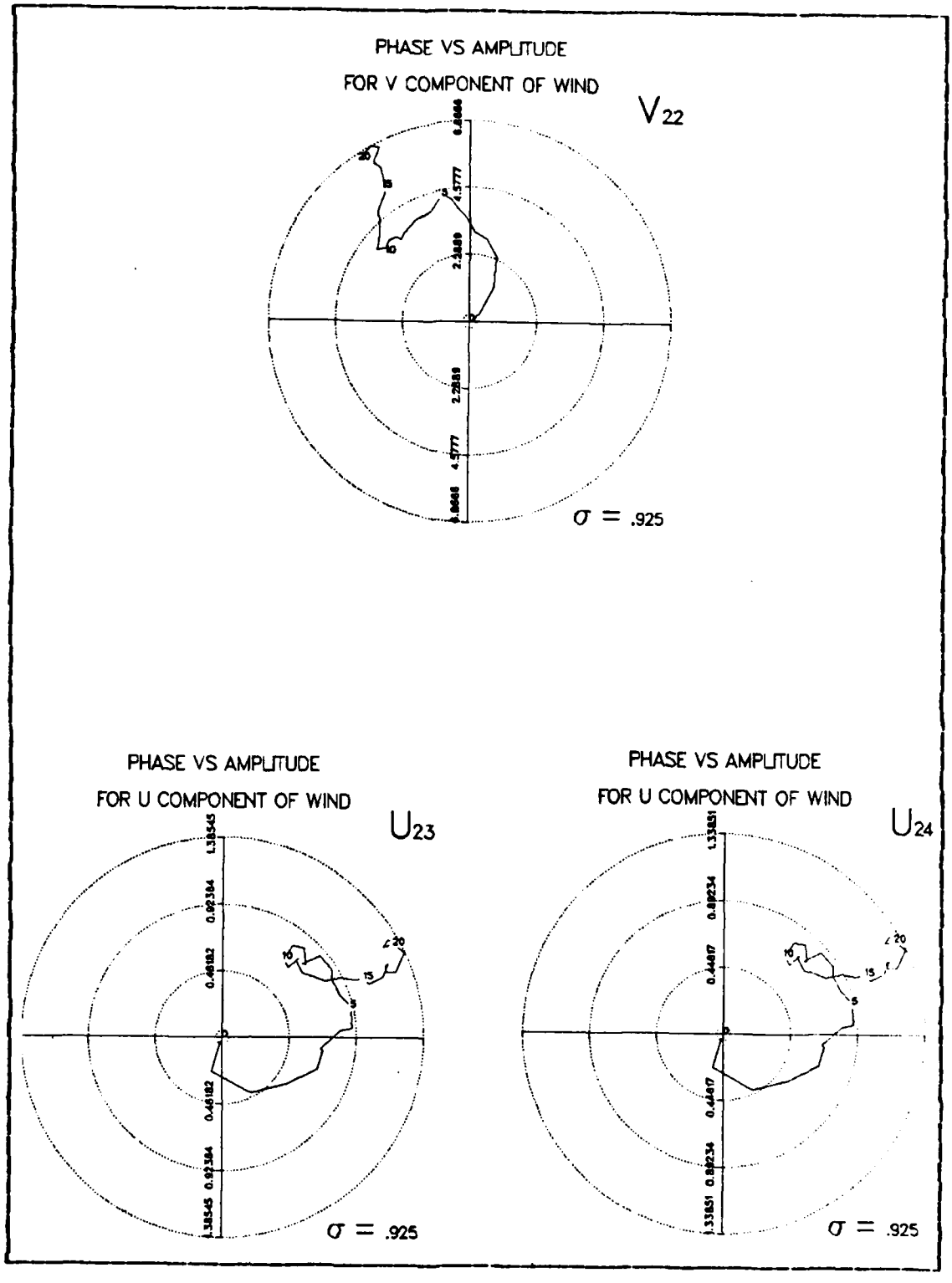

Figure 4.5 Harmonic Dials for Meridional(U) and Zonal(U) Wind Case 5.

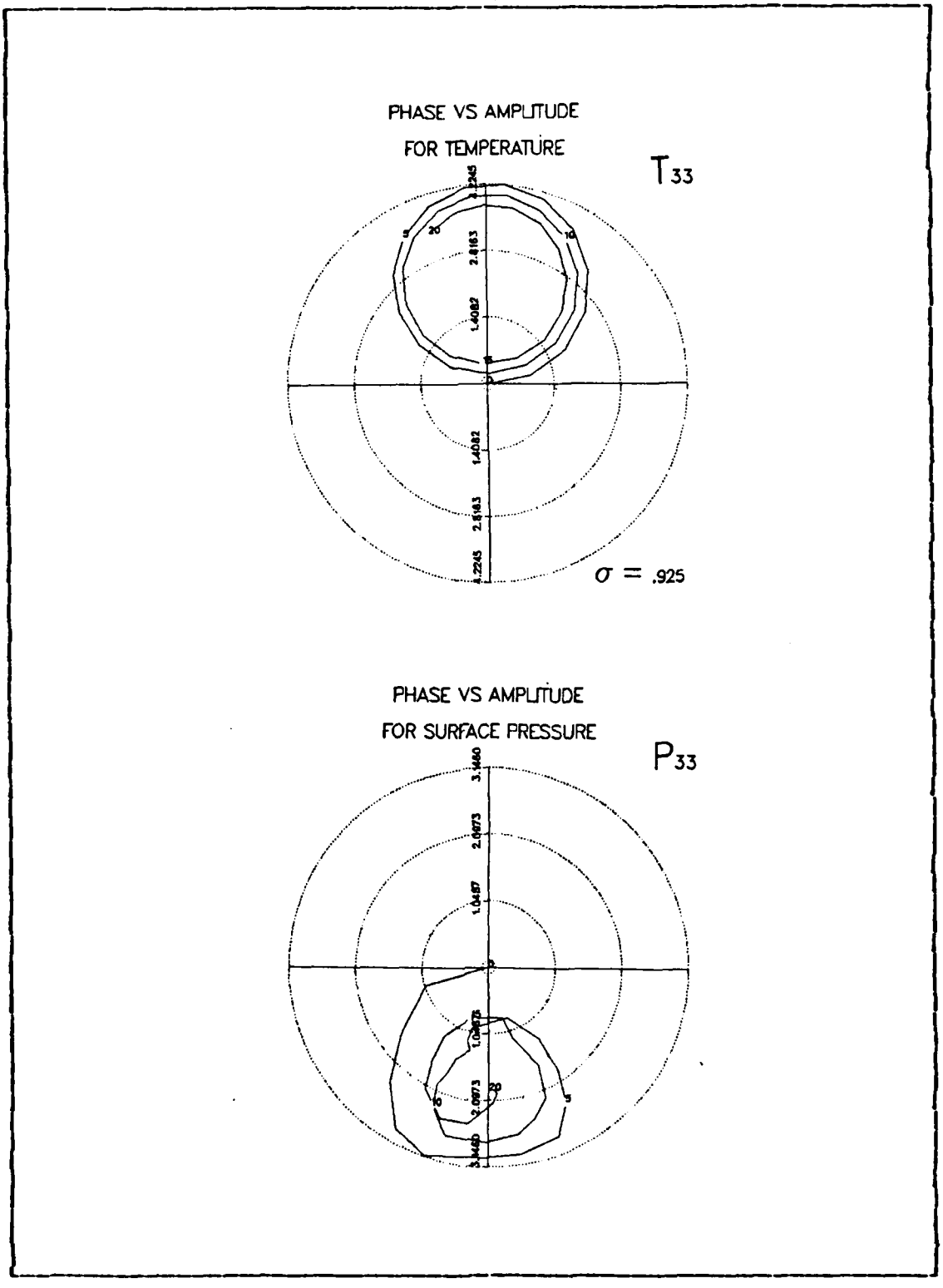

Figure 4.6 Same as Fig 4.4 for Case 6.

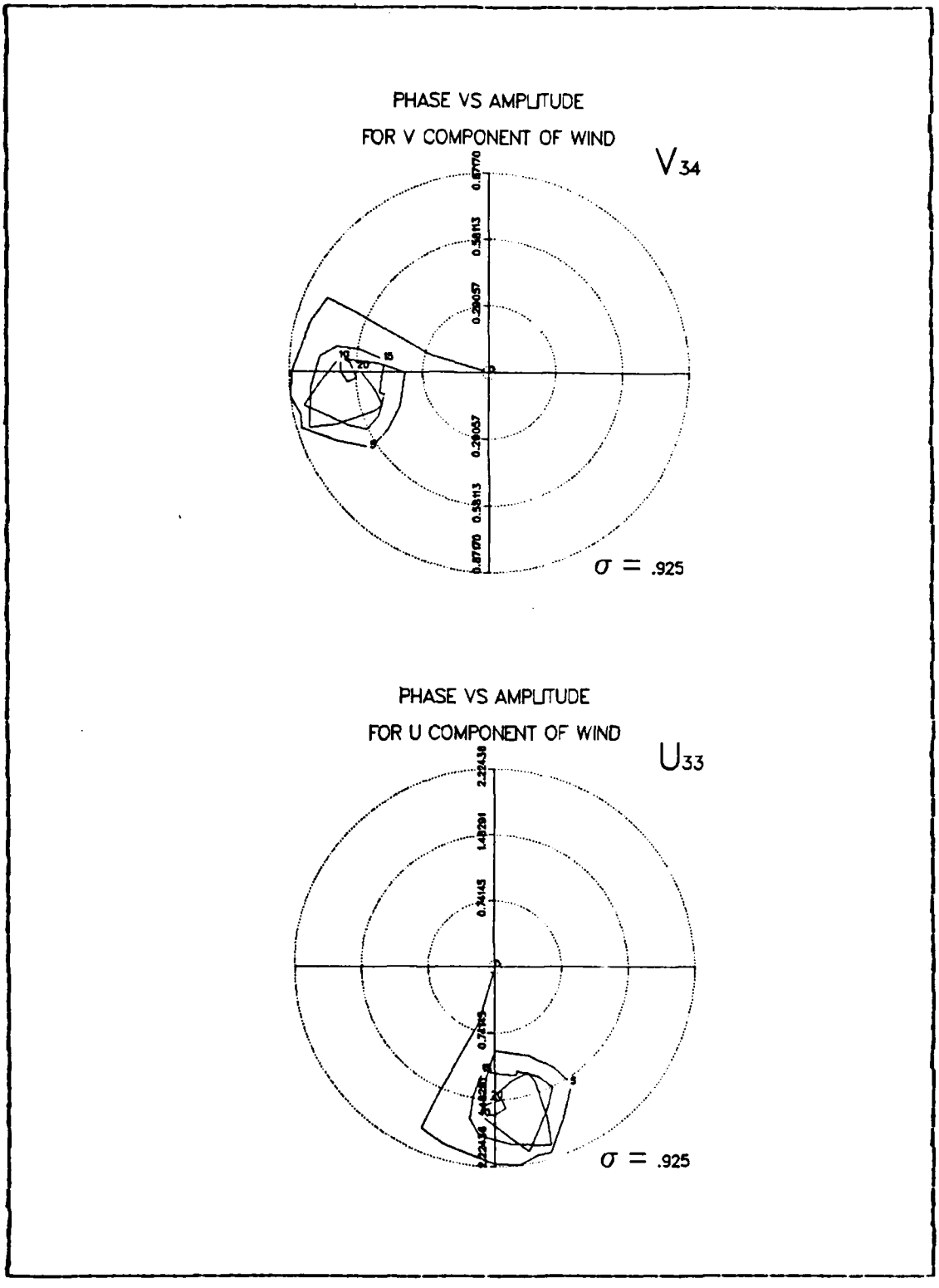

Figure 4.7 Same as Fig 4.5 for Case 6.

the three cases being considered. These estimates were obtained from Figs. 4.1 - 4.7 . Phase speeds were not calculated for the pressure and wind waves for case 5 due to the highly irregular nature of those dials. The phase speed of the temperature, pressure and wind waves are the same for wave component (3,3). Such is not the case for the other cases, though the phase speed are similar. The computed phase speed of the different variables for case 1 varies from 15.6 °/day for P to 18.5 °/day for U. The other cases have similar phase speeds for the different components. The general pattern which emerges from the data is that the phase speed of the transient components seems to be independent of wavenumber and that the waves are moving at approxi-

TABLE II

Period(p), and Phase Speed(c) for Transient Components

	Case 1		Case 5		Case 6	
	p	c	p	c	p	c
P	23.5	15.6	*	*	7.5	16.7
T	21.5	16.7	12.5	16.7	7.5	16.7
U	19.5	18.4	*	*	7.5	16.7
V	21.5	16.7	*	*	7.5	16.7

mately the speed of the mean wind(15.5 °/day). To test this hypothesis additional integrations were accomplished holding all other factors the same but increasing the speed of the mean wind. The results of these integrations showed an increase in phase speed of the component waves corresponding to the increase in the mean wind speed

A. STEADY STATE CASE

Since the purpose of this study was to see how sensitive the steady state solutions are to errors in the forcing and initial conditions it is important that the steady state

solutions of the model be examined to insure that they are indeed steady and that these sclutions are consistent with known theory.

To obtain steady state solutions the basic equations were integrated up to 30 days. It is obvious from Figs. 4.1-4.7 that after a rather lengthy integration the model atmosphere has yet not reached a steady state and that in fact the transient modes identified in the last section are clearly evident throughout the period of integration. Though there are indications that the solutions are slowly converging as indicated by the begining of spiral patterns in Figs. 4.1-4.7 a final steady state would not be reached for some time. However, by averaging over the period of the transient wave, it's effect can be averaged out. The remaining values are the steady state values. The above procedure was performed on case 1. To insure that the part of the solution which remained after averaging was truly the steady state solution another integration was performed using the averaged values as the initial conditions. Harmonic dials were again constructed for each of the variable wave components. If the fields obtained by averaging were truly the steady state solutions, one would expect to see no phase or amplitude change with time, i.e. the harmonic dial would collapse to a single point. Figs. 4.8 and 4.9 contain the harmonic dials from a 20-day integration initialized with the averaged values for case 1. The temperature wave is almost completely stationary, but the pressure and velocity components have small growth and movement. The fact that the pressure and wind component waves are not completely stationary is another indication that there are transient modes in these waves which are not contained in the temperature wave. Consequently, the averaging which was performed over the period of the temperature wave did not average out all of the transient parts of the pressure and wind waves.

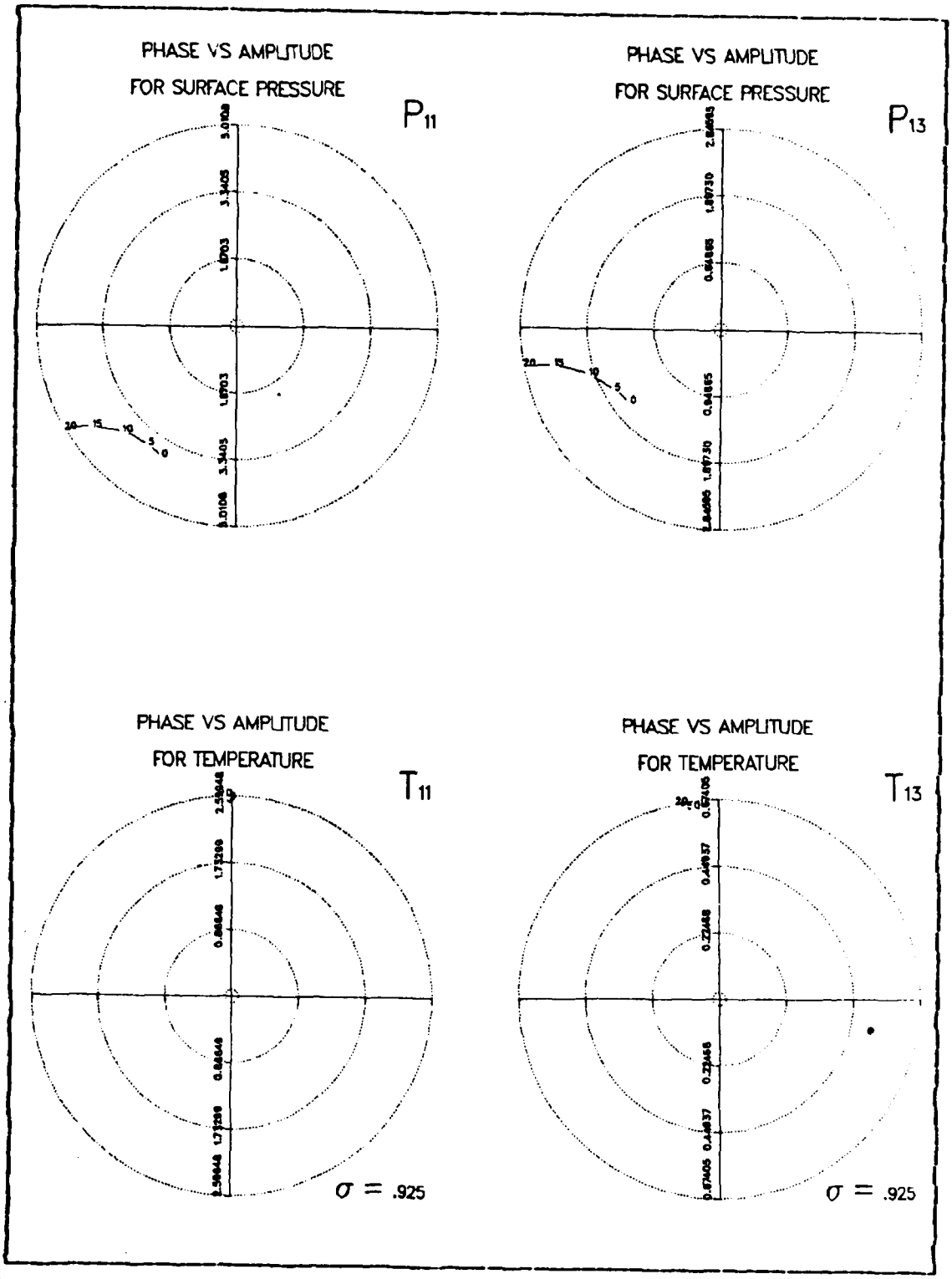

Figure 4.8 Same as Fig 4.2 for Steady State Initial Conditions.

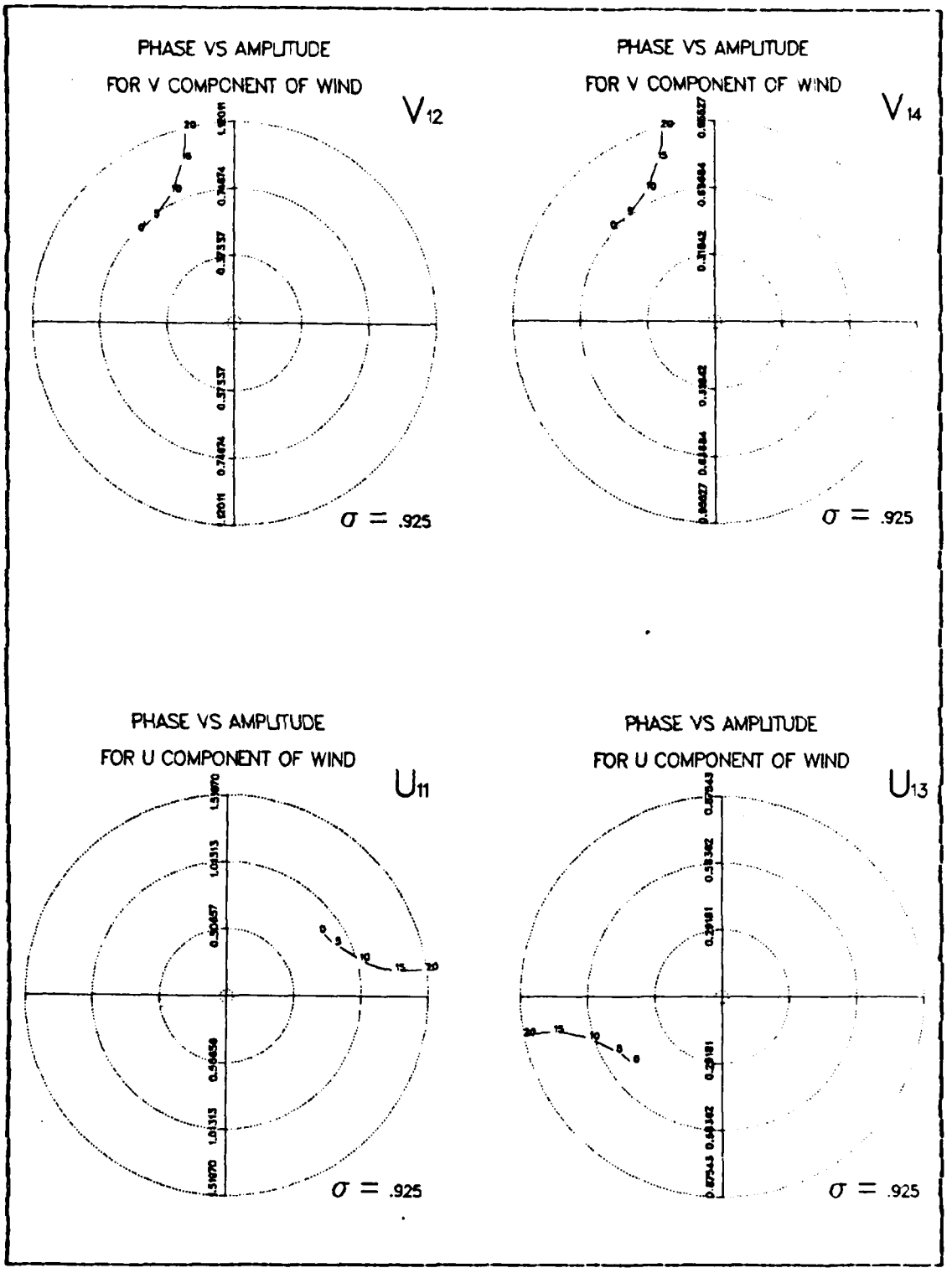

Figure 4.9 Same as Fig 4.3 for Steady State Initial Conditions.

It appears from the above integrations that solutions obtained by averaging over the period of the transient component are very close to steady state values. In order to better understand these solutions they will be compared to the steady state solutions from a simplified analytic model. This model will be derived in the next section.

B. THE ANALYTIC MODEL

The predictive system of equations for planetary scale motion in $Z=-\ln(P/P_0)$ coordinates are:

$$D+\frac{\partial \dot{Z}}{\partial Z} - \dot{Z} = 0 \tag{4.1}$$

$$\frac{\partial}{\partial t}\left(\frac{\partial \phi'}{\partial Z}\right)+\vec{V}\cdot\vec{\nabla}\frac{\partial \phi'}{\partial Z}+\dot{Z}\overline{\Gamma}(Z)+\dot{Z}\Gamma' = Q(Z) \tag{4.2}$$

$$\vec{V} = \frac{1}{f}\vec{k}\times\vec{\nabla}\phi \tag{4.3}$$

where

$$D = \vec{\nabla}\cdot\vec{V}$$

$$\dot{Z} = -\dot{p}/p$$

$$\phi = \overline{\phi}(Z)+\phi'(x, y, Z)$$

$$\Gamma = \frac{\partial}{\partial Z}\left(\frac{\partial \phi}{\partial Z} +\kappa\overline{\phi}\right) = \frac{H^2 g}{T}\left(\frac{g}{Cp} + \frac{1}{H}\frac{\partial \overline{T}}{\partial Z}\right)$$

$$H^2 = R\overline{T}/g$$

$$\Gamma' = \frac{H^2 g}{T}\left(\frac{g}{Cp} + \frac{1}{H}\frac{\partial T'}{\partial Z}\right)$$

Eq. 4.1 is the continuity equation, Eq. 4.2 is the first law of thermodynamics and Eq. 4.3 is the geostrophic relation. These equations were obtained by scaling the general baroclinic equations (Haltiner and Williams, 1980) with:

$L/a \sim 1 \quad R < .01 \quad \epsilon \sim 100 \quad \beta a/f \sim 1$

Where L is the horizonal scale, R is the Rossby Number and ϵ is a rotational Froude number. Assuming a steady state atmosphere ($\frac{\partial}{\partial t} = 0$) in solid rotation ($U = \omega a \cos\Psi$) and droping the $\Gamma'(Z)$ term, because it is small, Eq. 4.2 becomes:

$$\omega \frac{\partial}{\partial \lambda} \frac{\partial \phi'}{\partial Z} + \bar{\Gamma} \dot{Z} = Q(Z) \tag{4.4}$$

The meridional and zonal components of the geostrophic wind in spherical coordinates are:

$$V = \frac{1}{2a\Omega \cos\Psi \sin\Psi} \frac{\partial \phi'}{\partial \lambda} \tag{4.5}$$

$$U = - \frac{1}{2a^2\Omega \sin\Psi} \frac{\partial \phi'}{\partial \Psi} \tag{4.6}$$

Using Eqs. 4.5 and 4.6 the divergence in spherical coordinates can be written:

$$D = \frac{2\Omega \cos\Psi}{2a\Omega \sin\Psi} = - \frac{\beta V}{f} \tag{4.7}$$

Now Eq. 4.1 can be written:

$$\frac{\partial \dot{Z}}{\partial Z} - \dot{Z} - \frac{1}{a^2\Omega \sin^2\Psi} \frac{\partial \phi'}{\partial \lambda} = 0 \tag{4.8}$$

Assuming solutions of the form:

$$\phi' = \Phi(Z) e^{im\lambda} P_n^m(\Psi) \tag{4.9}$$

$$\dot{Z} = W(Z) e^{im\lambda} P_n^m(\Psi) \tag{4.10}$$

$$Q = N(Z) e^{im\lambda} P_n^m(\Psi) \tag{4.11}$$

Eq. 4.4 and 4.8 become:

$$\omega i m \Phi(Z) + \Gamma W(Z) = N(Z) \tag{4.12}$$

$$W' - W - \frac{im\Phi}{a^2\Omega\sin^2\Psi} = 0 \qquad (4.13)$$

Eq. 4.12 and 4.13 can be combined to obtain a single equation for W

$$\omega a^2\Omega\sin^2\Psi(W''-W')+\Gamma W = N \qquad (4.14)$$

Eq. 4.14 is just a 2nd order nonhomogenous ordinary differential equation for W whose general solution is of the form:

$$W = C_1W_1+C_2W_2+W_p$$

Where W_1, W_2 are the solutions to the homogeneous part of Eq. 4.14 and W_p is the particular solution. Assuming $N(Z) = N_0e^{-\alpha^2 Z}$, the solution to Eq. 4.14 is

$$W = C_1e^{r_+Z}+C_2e^{r_-Z}+Ae^{-\alpha^2 Z} = e^{Z/2}(C_1e^{q^2 Z}+C_2e^{-q^2 Z}) \qquad (4.15)$$

where

$$r_\pm = \frac{1}{2} \pm\sqrt{1/4-\Gamma/\omega a^2\Omega\sin\Psi} = \frac{1}{2} + q^2$$

α^2 = some positive number

$$A = N_0/(\omega a^2\sin^2\Psi(\alpha^4+\alpha^2)+\Gamma)$$

There are two possible solution cases for the homogeneous part of Eq. 4.14. If q^2 is positive the solution consists of an exponentially growing and decaying part. After applying the boundary conditions $w(0)=0$ and finite energy at $Z=\infty$, i.e. $(\rho|\phi|^2) = e^{-Z}|\phi|^2$ the solution becomes

$$W(Z) = A(e^{-\alpha^2 Z}-e^{Z/2}e^{-q^2 Z}) \qquad (4.16)$$

An expression for $\Phi(z)$ can be obtained by substituting Eq. 4.16 into Eq. 4.13

$$\Phi(Z) = -a^2\Omega\sin^2\Psi A\{e^{rZ}(r-1)+e^{-\alpha^2 Z}(1+\alpha^2)\} \quad (4.17)$$

If q^2 is negative the solution will be oscillatory in Z and of the form

$$W(Z) = e^{Z/2}(C_1 e^{-i\mu Z}+C_2 e^{i\mu Z})+Ae^{-\alpha^2 Z} \quad (4.18)$$

where

$$\mu = \sqrt{\Gamma/\omega a^2\Omega\sin^2\Psi - 1/4} \quad (4.19)$$

After applying the radiation boundary condition at $Z=\infty$ i.e. $w(Z)$ $\phi(Z)>0$ and the lower boundary condition $w=0$ at $Z=0$ Eq. 4.18 becomes

$$W(Z) = A\{(\frac{3}{2}i-\mu)e^{(\frac{1}{2}+i\mu)Z}-i(-1-\alpha^2)e^{-\alpha^2 Z}\} \quad (4.20)$$

The corresponding expression for (z) is

$$\Phi(Z) = a^2\Omega\sin^2\Psi A\{(\frac{3}{2}i-\mu)e^{(\frac{1}{2}+i\mu)Z}-i(-1-\alpha^2)e^{-\alpha^2 Z}\} \quad (4.21)$$

Eqs. 4.16,4.17 and Eqs. 4.20,4.21 can be substituted into Eqs. 4.9 and 4.10 to obtain expressions for $\phi$and $\dot{Z}$. After taking the real part the $q^2 > 0$ solution are

$$\phi' = a^2\Omega\sin^2\Psi A\{e^{rZ}(r-1)+e^{-\alpha^2 Z}(1+\alpha^2)\}\sin(m\lambda)P_n^m \quad (4.22)$$

$$\dot{Z} = A(e^{-\alpha^2 Z}-e^{rZ})\cos(m\lambda)P_n^m \quad (4.23)$$

The $q^2 < 0$ solutions are

$$\phi' = a^2\Omega\sin^2\Psi A\{e^{Z/2}(\frac{3}{2}\sin(\mu Z+m\lambda) \quad (4.24)$$

$$+\mu\cos(\mu Z+m\lambda)+(1+\alpha^2)e^{-\alpha^2 Z}\sin(m\lambda)\}P_n^m$$

$$\dot{Z} = A\{e^{-\alpha^2 Z} - (e^{Z/2}\cos(\mu Z))\cos(m\lambda) \qquad (4.25)$$

$$+(e^{Z/2}\sin(\mu Z))\sin(m\lambda)\, P_n^m$$

If $q^2 > 0$ the response of the atmosphere to heating is trapped near the surface and the vertical structure is one in which the waves have no tilt with height. If $q^2 < 0$ the perturbation due to the heating will radiate to great heights and the waves will tilt westward. In both cases the steady state represents a balance between advection, adiabatic warming(cooling) and diabatic heating(cooling). The longitudinal and latitudinal structure, for each case, will be determined by the forcing specified. That is, if wavenumber one is specified in the forcing term, the steady state solution will have a wave one form. In addition, since the winds are geostrophic their structure will be determined by the structure of ϕ'. Eq. 4.24 can be written

$$\phi' = -A\{(\tfrac{3}{2}e^{Z/2}\sin(\mu Z) - e^{Z/2}\mu\cos(\mu Z))\cos(m\lambda) \qquad (4.26)$$

$$+(\tfrac{3}{2}e^{Z/2}\cos(\mu Z) - \mu e^{Z/2}\sin(\mu Z) - (1+\alpha^2)e^{-\alpha^2 Z})\sin(m\lambda)\}P_n^m$$

which can be written in the form

$$\{G(Z)\cos(n\lambda + H(Z))\}A(\Psi)P_n^m(\Psi) \qquad (4.27)$$

This form allows comparison with the phase and amplitude of the model Legendre functions. If the model steady state solutions really are steady state one would expect them to at least qualitatively agree with the analytic solutions derived above. The differences between the numerical model atmosphere and the analytic atmosphere are:

1. A nondimension vertical coordinate Z is used in the analytic model while sigma coordinates are used in numerical model,
2. Friction is not included in the analytic model, and

3. $\Gamma(Z)$ is assumed to be constant in the analytic model while it is not in the numerical model.

$\Gamma(Z)$ is not constant in the numerical model because $\Gamma(z)$ is constant. The fact that $\Gamma(Z)$ is not constant given $\Gamma(z)$ is can be shown by examining the eguation for $\Gamma(Z)$

$$\Gamma(Z) = \frac{H^2 g}{T}\left(\frac{g}{Cp} + \frac{1}{H}\frac{\partial T}{\partial Z}\right) \qquad (4.28)$$

After converting to z coordinates Eq. 4.28 becomes

$$\frac{H^2}{T}\left(\frac{g}{Cp} + \frac{\partial T}{\partial Z}\right) \qquad (4.29)$$

Since the lapse rate is a constant 6.5 °/Km in the model the second term in Eq. 4.29 is constant but T decreases with z so the first term is not constant thus $\Gamma(Z)$ will not be constant in the model atmosphere. However, since the decrease in temperature is rather small compared to the mean temperature $\Gamma(Z)$ is nearly constant so that qualitative comparisons are still possible. In addition, the vertical structure of the forcing in the analytic model is a simple exponential form $e^{-\alpha^2 Z}$ while in the model it is of the form $e^{\frac{\sigma-1}{.3}} = e^{\frac{P-P_S}{300}}$. However, given that is chosen such that the e-folding depth of $e^{-\alpha^2 Z}$ is the same as that for $e^{\frac{P-P_S}{300}}$ then the two functions will be similar except for the upper levels where both functions are small and have little effect on the total solution. Fig. 4.10a is a plot of the numerical model forcing vertical structure where P_S is assumed to be constant and equal to 1000mb. This is not a bad assumption because the model contains no topography and the maximum pressure perturbaticns are only a few millibars. This assumption also allows qualitative comparisons between variables in and P coordinates. The e-folding depth here occurs at P=700mb. For P=700 , Z=-ln(700/1000)=-ln(.7). Thus, to have the same folding depth α^2 must be choosen to

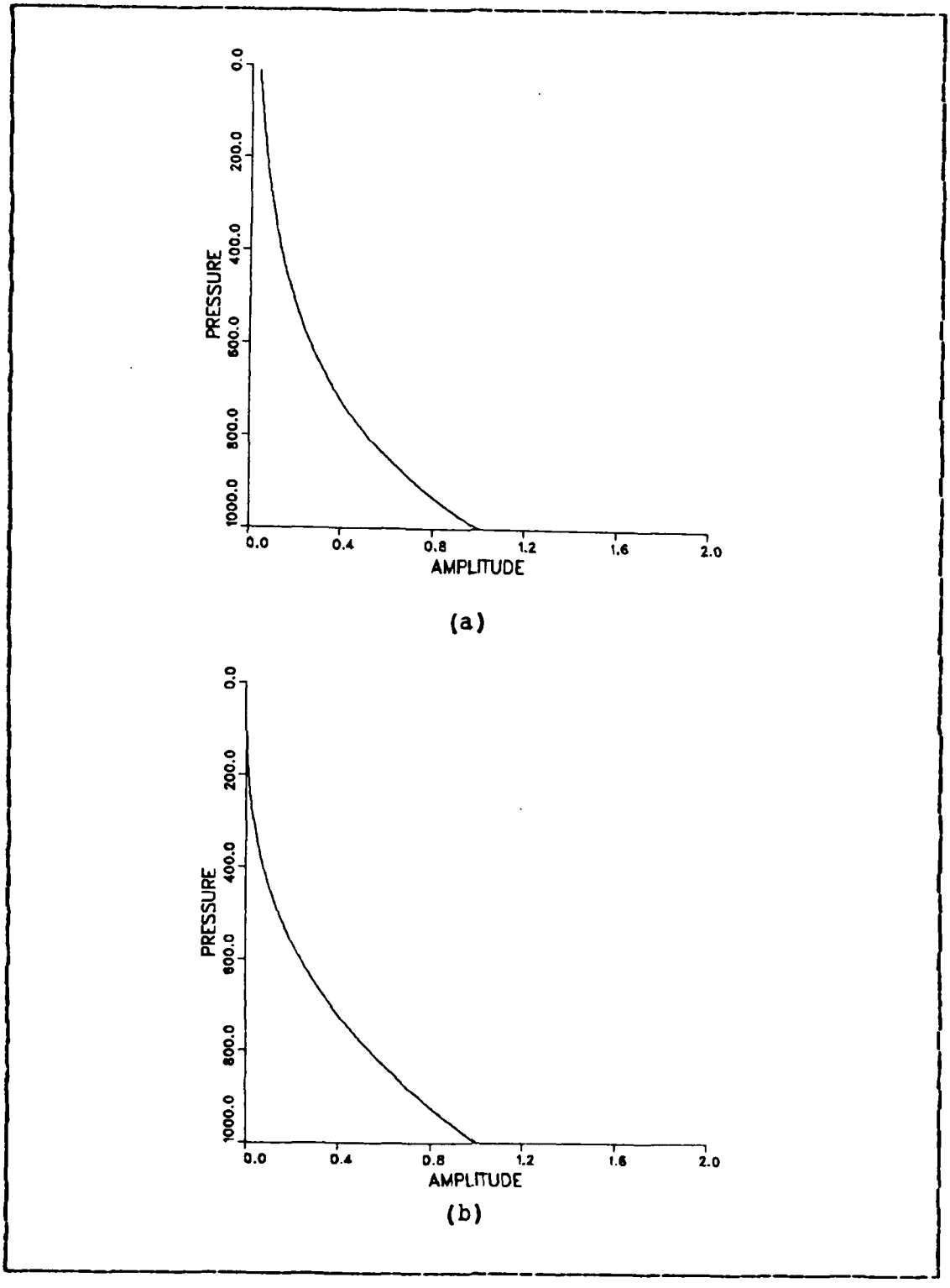

Figure 4.10 Heating Vertical Structure (a) Numerical model and (b) Analytic.

be equal to 1/(-ln.7). Fig. 4.10b is a plot of $e^{-\alpha^2 Z}$ converted to P coordinates. Note that the plots are very similar up to 400mb. Figs. 4.11a and 4.11b are plots of G(Z) and H(Z) vs pressure using the following estimate for the various parameters in Eq. 4.19: $\omega = (20\ m/s)/a$, $\Gamma \sim (Z)$ H^2N^2, H=10km, $N^2=10^{-4}s^{-1}$, $a=6.37 \times 10^6$ m and $\Omega = 7.292 \times 10^{-5}s^{-1}$. Figs. 4.12 and 4.13 contain plots of the steady state model solutions for the meridional (V) and zonal (U) wind vs sigma for case 1. Since the winds are geostrophic the vertical structure U and V can be compared with the vertical structure of ϕ. Note the striking similarities between the two sets of figures. Both amplitude plots show a slight decrease in the lower layers and an exponential increase near the top of the atmosphere. Also, given Figs. 4.14, 4.15 and 4.16, it is obvious that the model's steady state solutions have the longitudinal wave one form specified in the case 1 forcing term. These figures are horizontal cross-section for vorticity, meridional velocity and temperature near the top and bottom of the model atmosphere. Contour intervals are indicated at the top of each cross-section. The vertical scale at the bottom of the figures is used to represent topography, which is not included in this model. It is clear that the steady model solutions are qualitatively consistent with the analytic solutions and that the method used to determine these values was a sound one. The question might now be asked why are the model solutions oscillatory in nature? Is it not possible that they could be of the exponential decaying type? These questions can be answered by examining Eq. 4.19 more closely. Given that

$$\Gamma/\omega a^2 \sin^2\Psi > \frac{1}{4} \qquad (4.30)$$

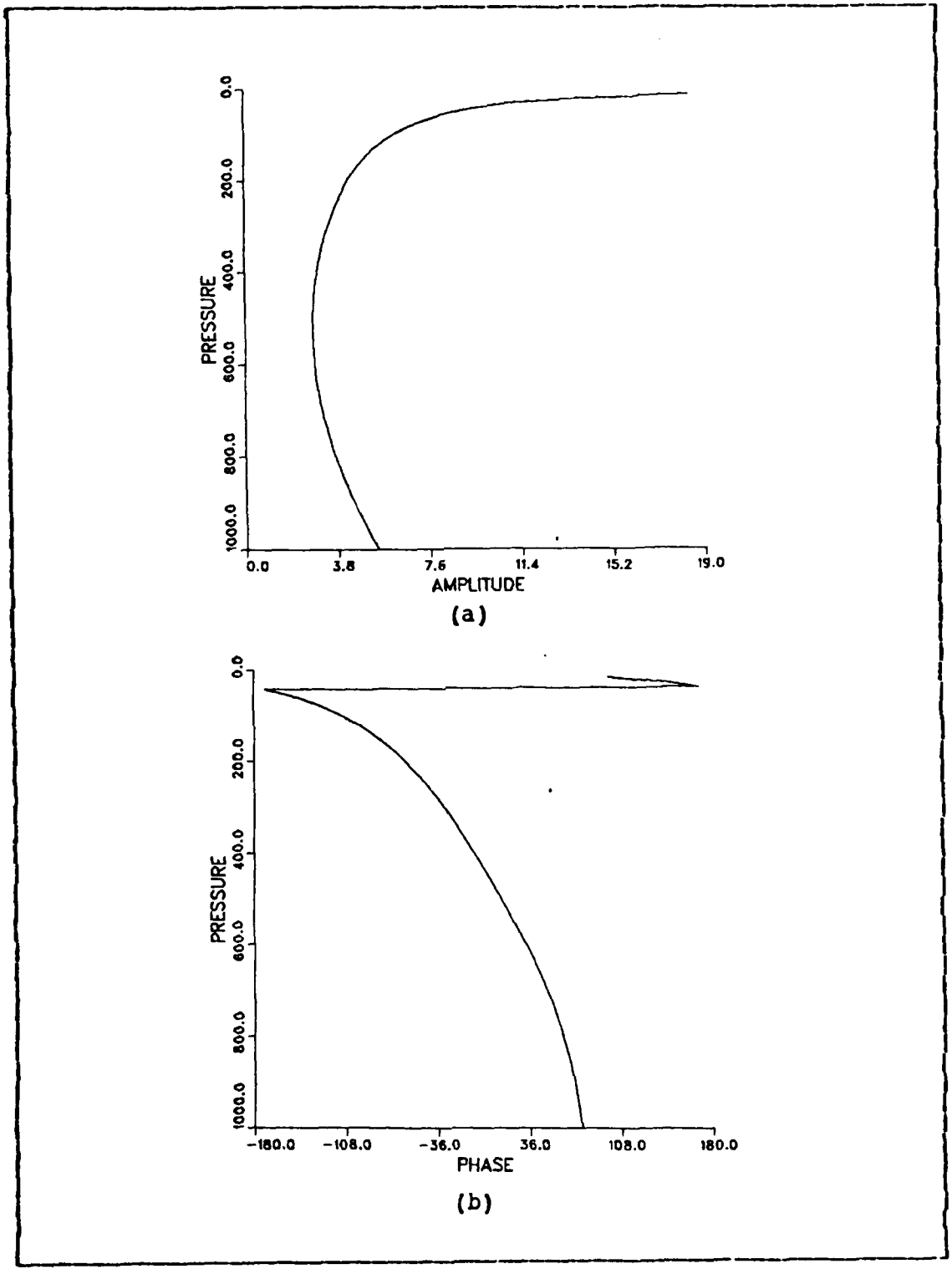

Figure 4.11 Analytic Vertical Structure
(a) Amplitude and (b) Phase.

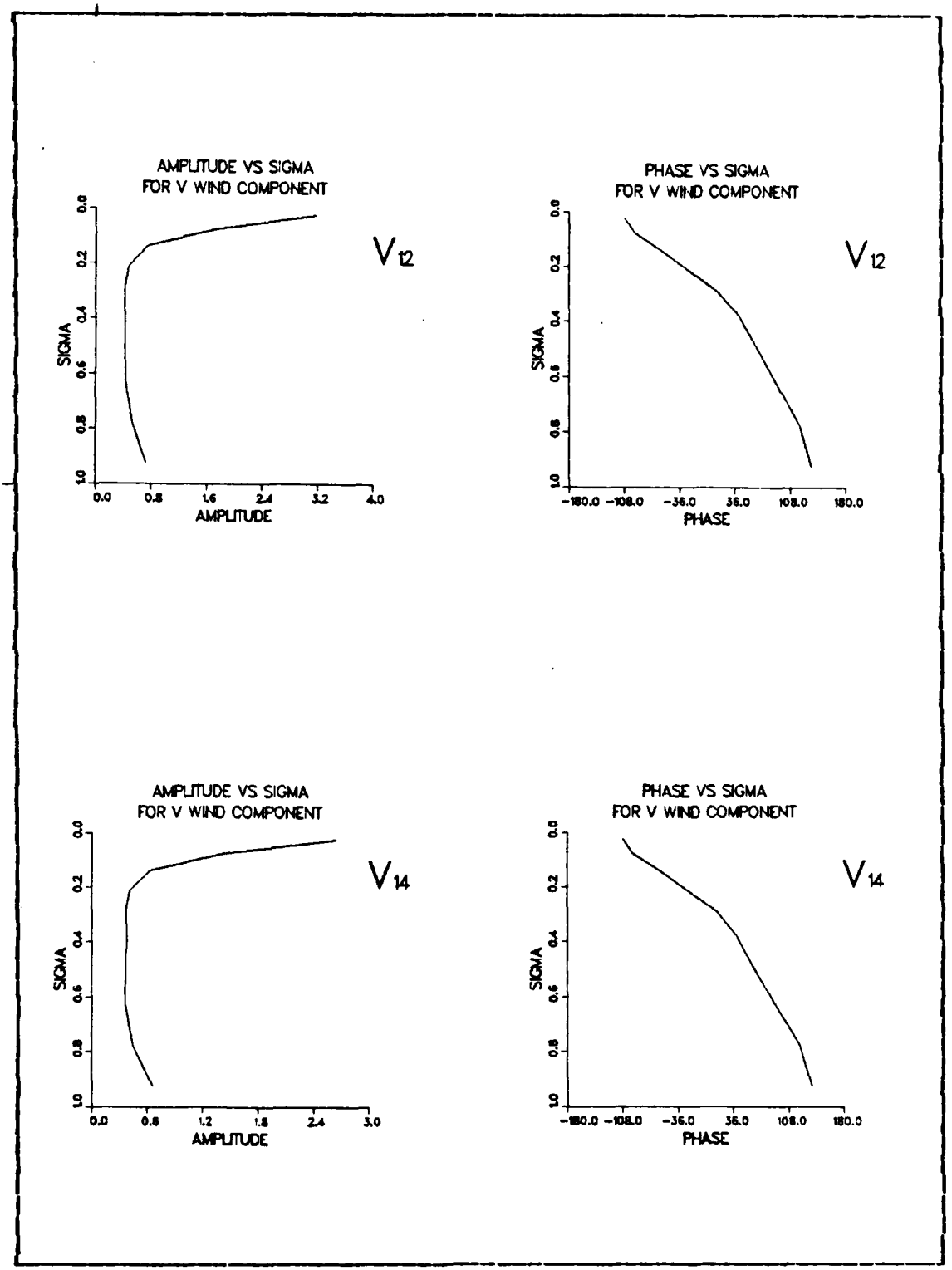

Figure 4.12 Model Vertical Amplitude and Phase Structure for Case 1.

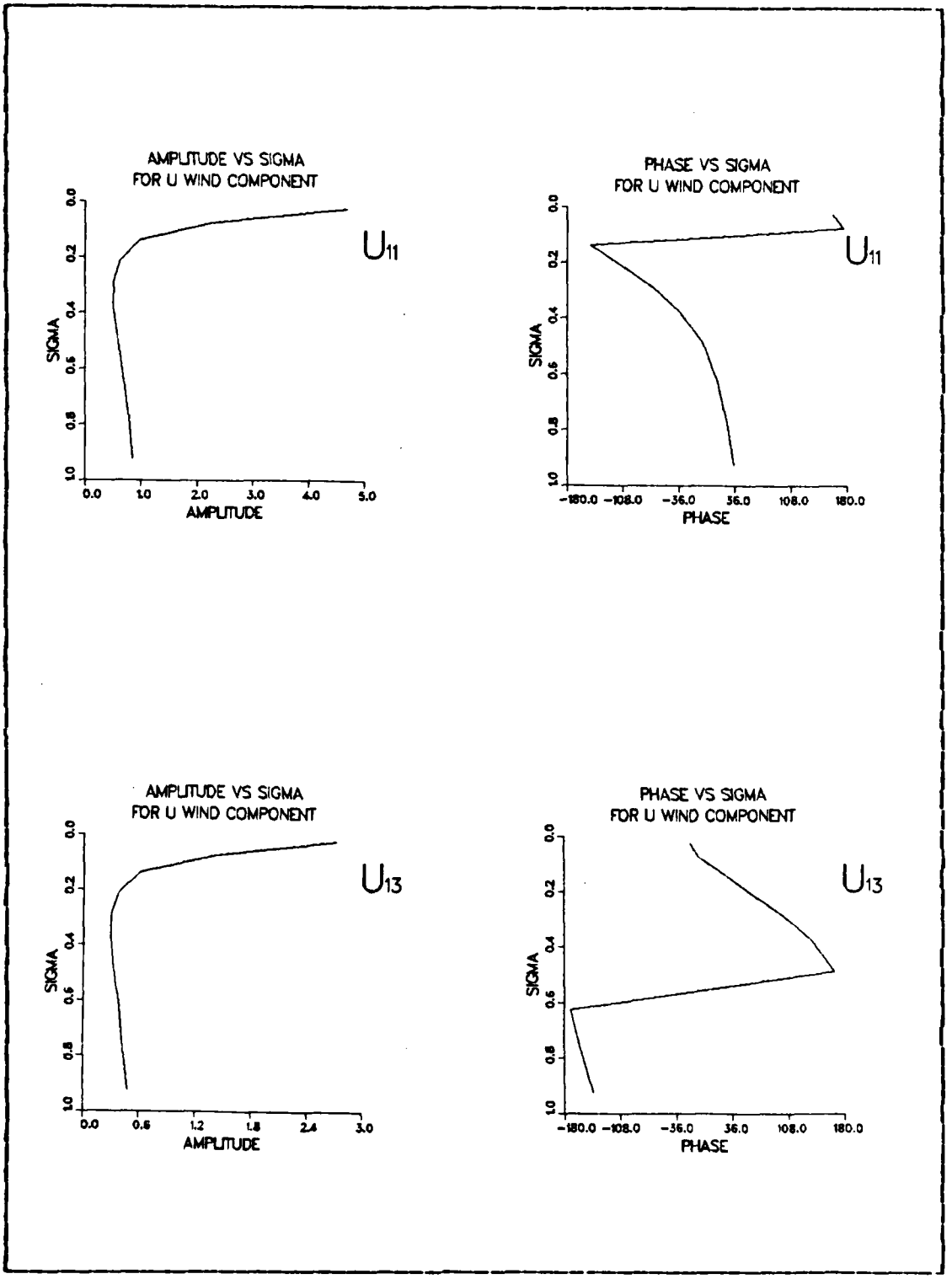

Figure 4.13 Model Vertical Amplitude and Phase Structure for Case 1.

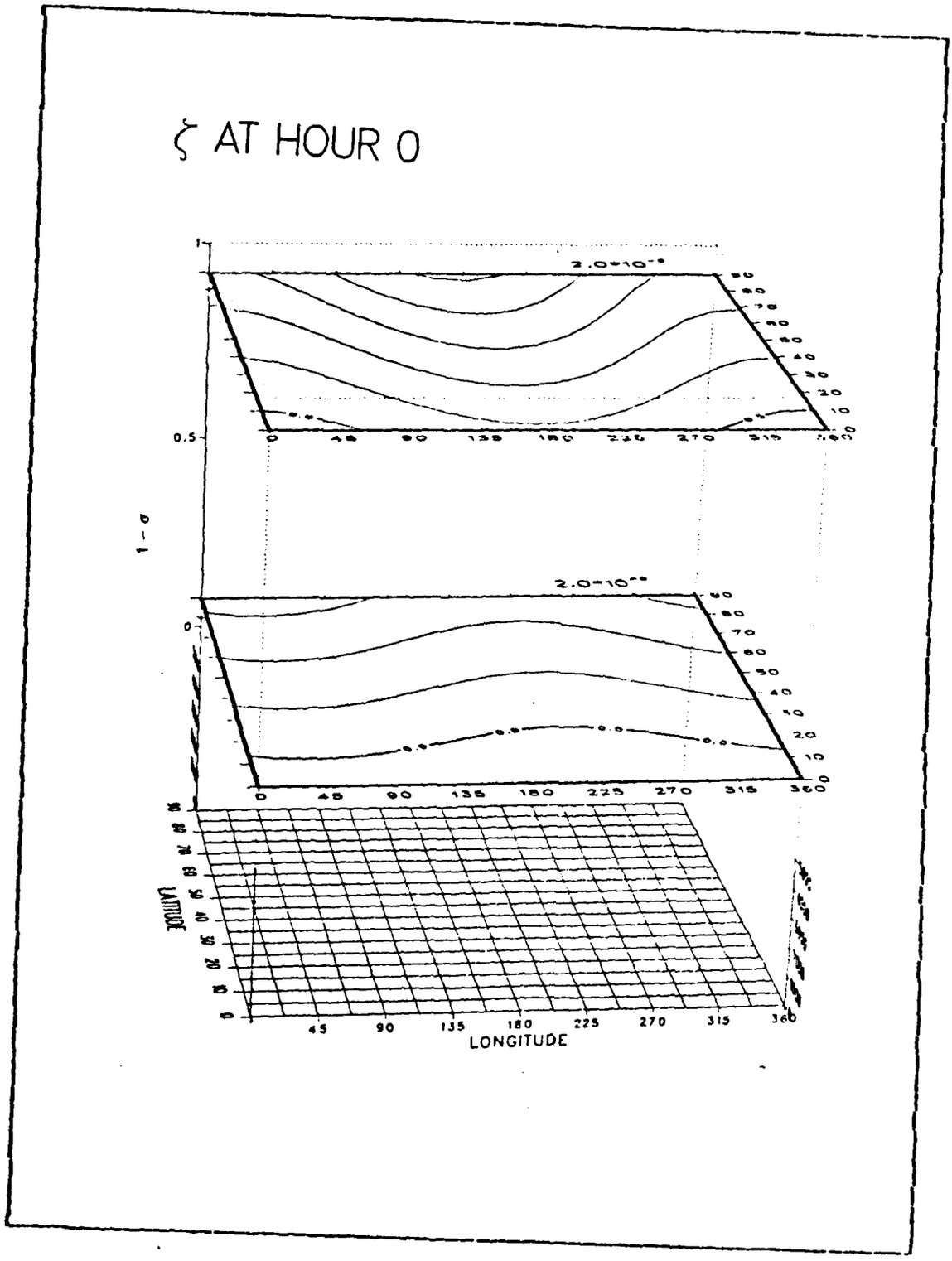

Figure 4.14 Steady State Longitudinal Vorticity Structure for Case 1.

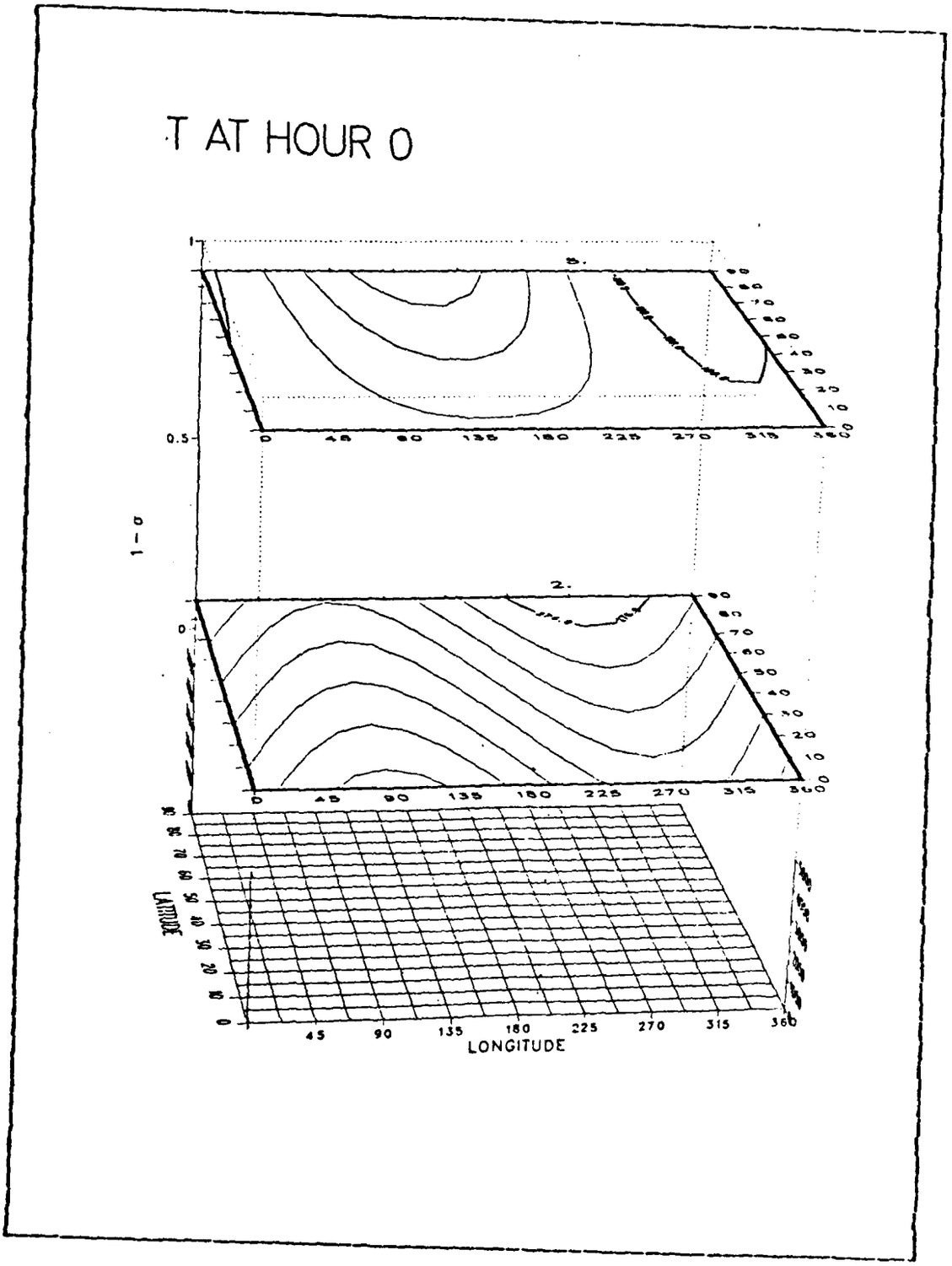

Figure 4.15 Steady State Longitudinal Temperature Structure for Case 1.

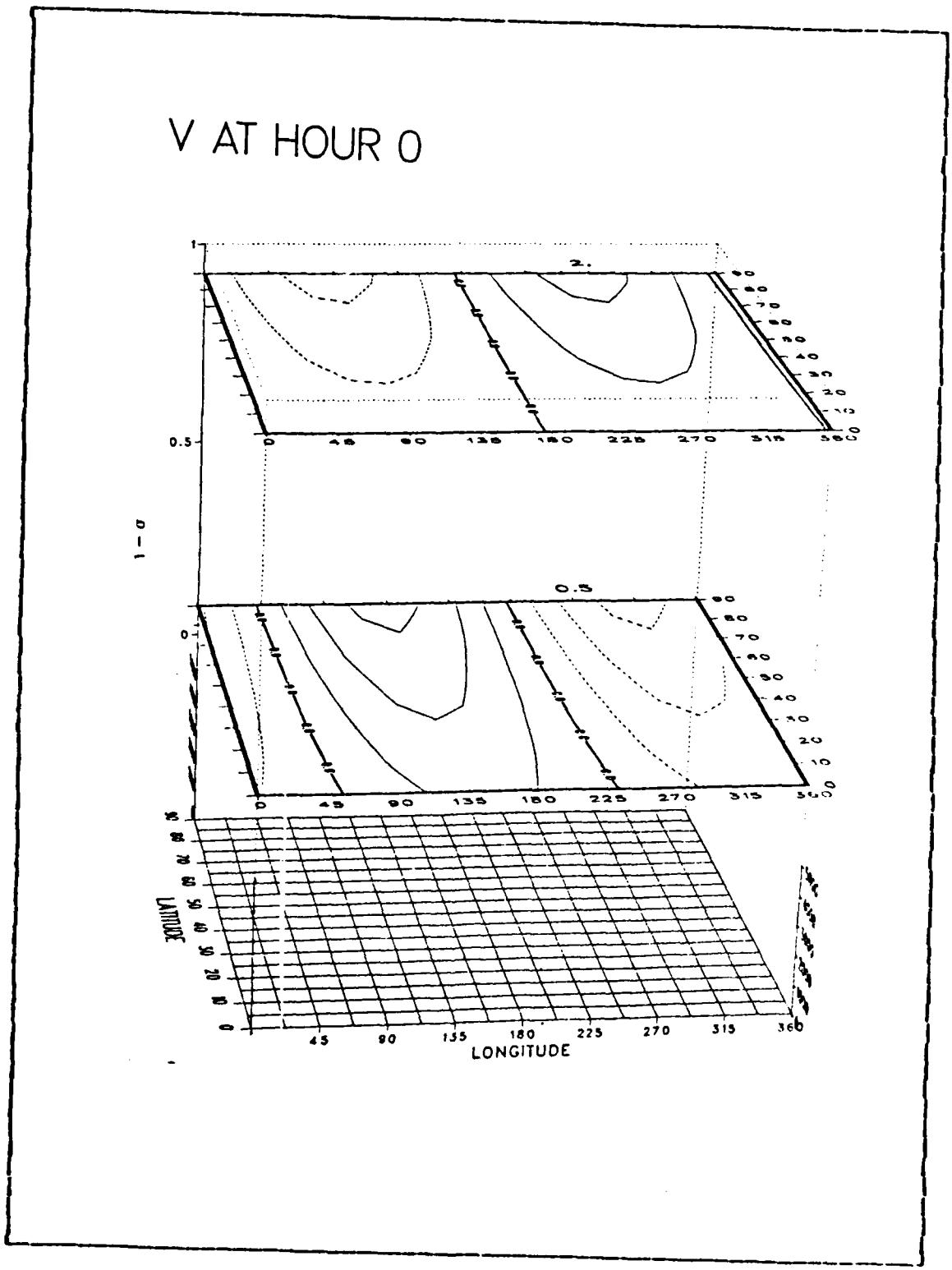

Figure 4.16 Steady State Longitudinal V Velocity Structure for Case 1.

the solution will be oscillatory. In the model, ω is specified so that the zonal wind is equal to 20 m/s at the equator so that $U=\omega a \cos \quad =U=\omega a$ at $\quad =0$ thus $\omega=U/a$. Given $\Gamma \sim H^2 N^2$, $H \sim 10$ km, $N^2 = 10^{-4} s^{-1}$, $a = 6.37 \times 10^6$ m, $\Omega = 7.292 \times 10^{-5} s^{-1}$ one can try to solve for a latitude where the solution will no longer be oscillatory. After using the above values Eq. 4.30 becomes

$$\sin\Psi = 20.84 \qquad (4.31)$$

which has no solution. Thus there is no point where the solution would not be oscillatory. To obtain non-oscillatory solutions one would have to increase the zonal wind speed to almost 100 m/s. Using these steady state solutions it is now possible to examine the sensitivity of these solutions to changes in the forcing and initial conditions.

C. SENSITIVITY EXPERIMENTS

Using the steady state solutions from case 1 as initial conditions two additional experiments are carried out to determine the sensitivity of the planetary waves to 'errors' in the forcing or initial conditions. In the first experiment errors are introduced in the forcing field. In fact a 100% error was introduced by turning off the forcing altogether. The model is then integrated out to 20 days. Figs. 4.17 and 4.18 contain the harmonic dials for the above integration. Note that for the most part the once quasi-stationary solutions are now almost purely transient since the phase through the entire range of phase. In the previously observed pattern the stationary plus transient nature of the waves was indicated by a change of phase and amplitude which occured in a particular quadrant of the dial.

The estimated phase speeds obtained from Figs 4.17 and 4.18 show these transient waves to again be moving at the speed of the mean wind. The fact that the waves are pure transient now is not surprising since the heating is no longer present to fix the wave to a particular location.

In the second experiment errors are introduced into the rotational part of the steady state wind by reducing those components by 20%. The model is again integrated out to 20 days. Figs. 4.19 and 4.20 contain the harmonic dials for this integration. From these figures one can see that the only wave which is moving eastward is the temperature wave. All the other component waves are moving westward. The temperature wave has a phase speed of about 12 °/day at the equator which is about 25% slower than the mean wind. It is evident that the e are a number of high frequency components present in the other component waves which are not present in the temperature wave. Since there is no simple circular pattern for the wind and pressure waves it is difficult to obtain the period of the transient part of the solution. The exact phase speed of these wave is not important. The important thing to note here is that the waves are moving slowly westward.

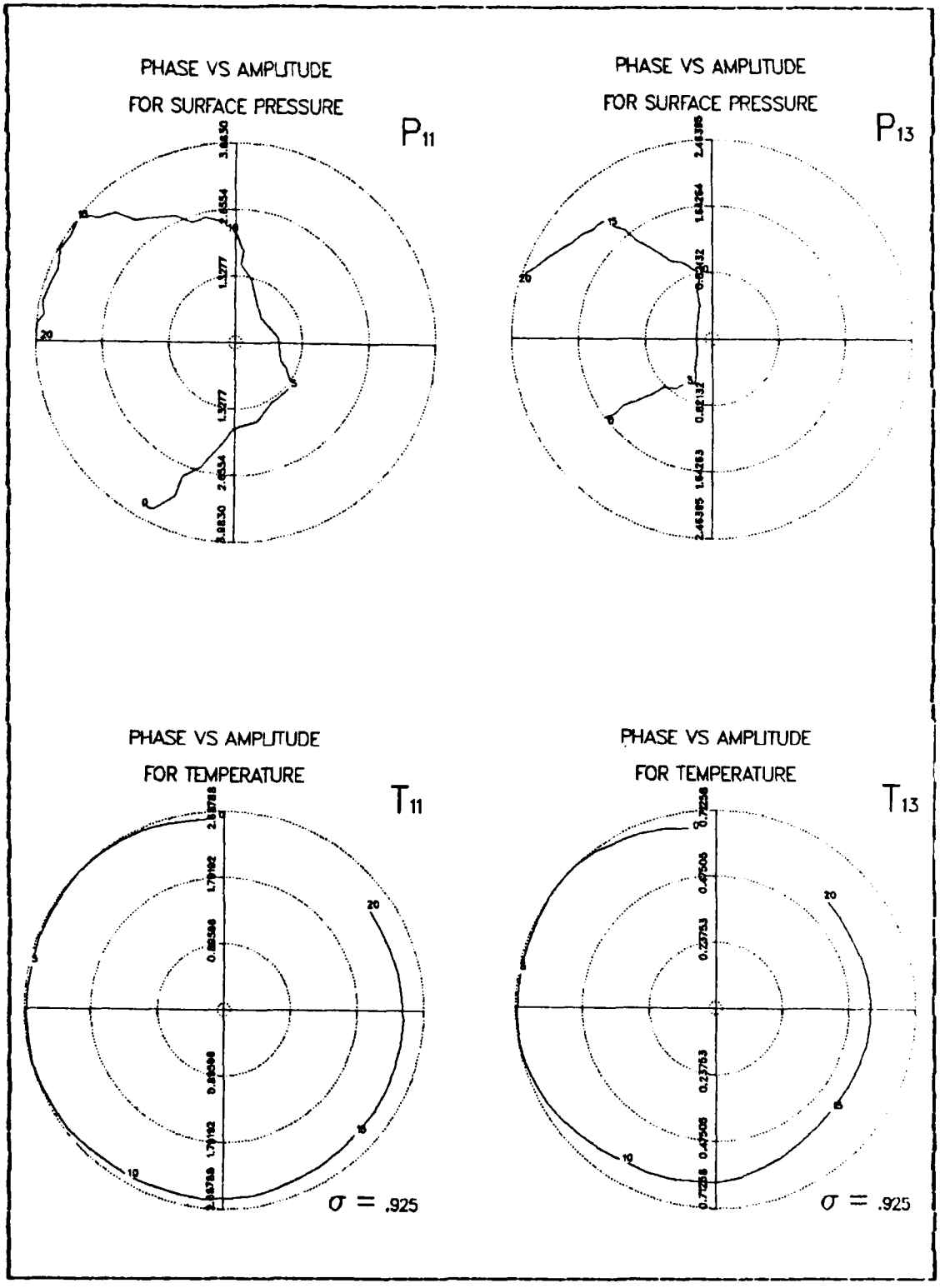

Figure 4.17 Same as Fig 4.2 for the Case with No Heating.

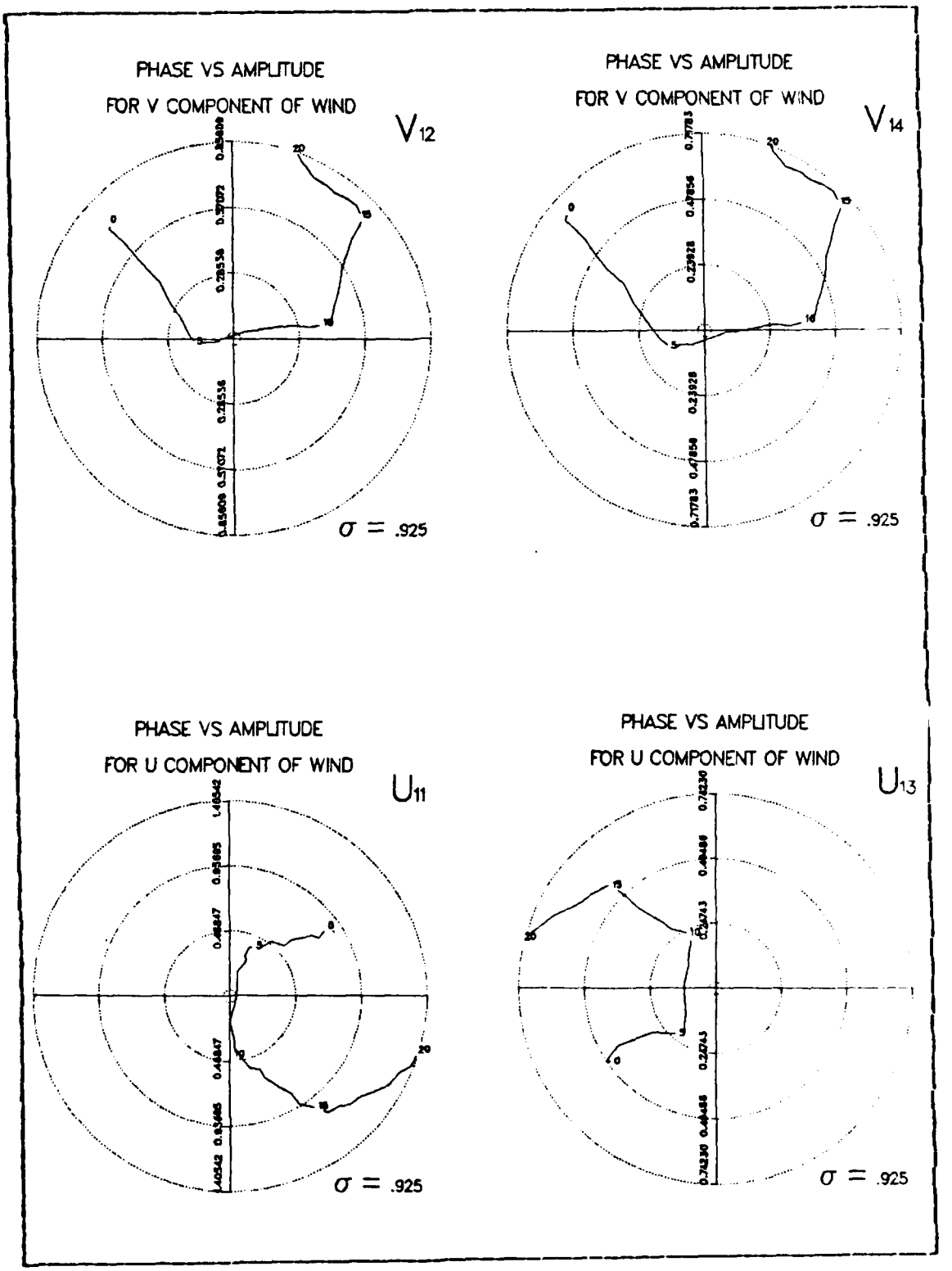

Figure 4.18 Same as Fig 4.3 for the Case with No Heating.

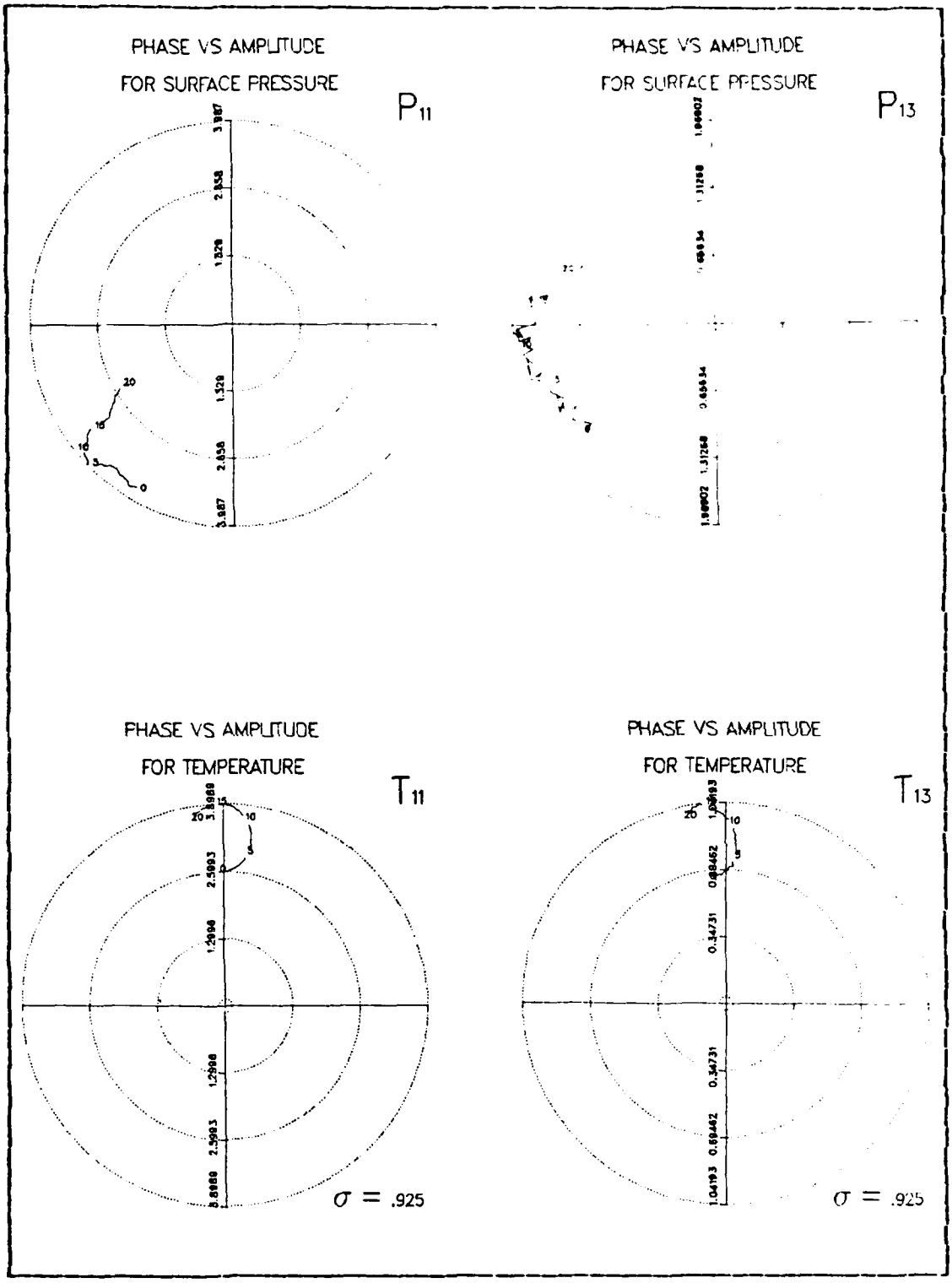

Figure 4.19 Same as Fig 4.2 for the Case with Rotational Wind Errors.

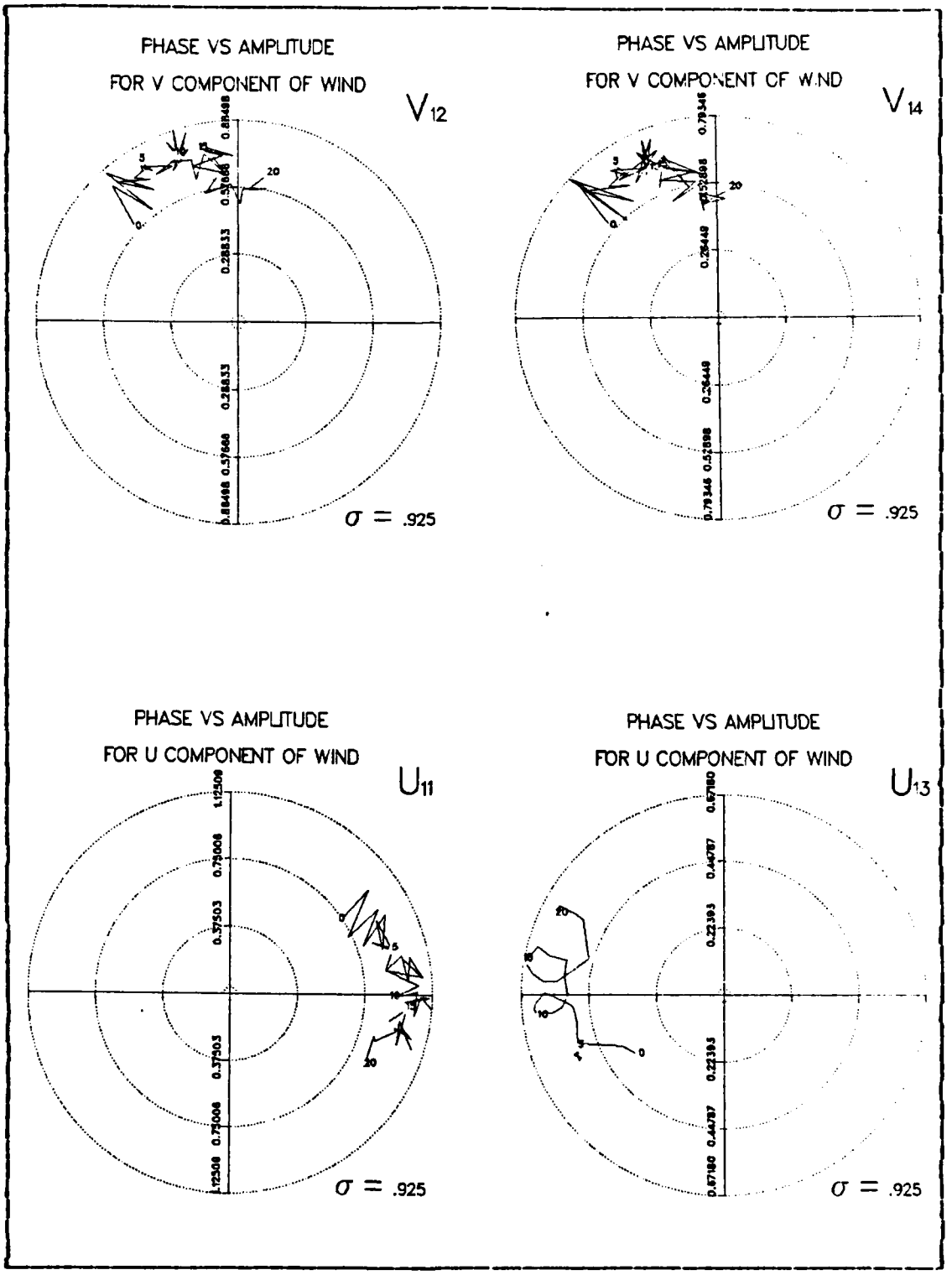

Figure 4.20 Same as Fig 4.3 for the Case with Rotational Wind Errors.

V. DISCUSSION AND CONCLUSIONS

The results of the previous section are best discussed in terms of normal mode theory. A number of investigators (Geisler and Dickinson, 1976, Daley et al, 1981, and Kasahara 1976) have used this method to examine the transient part of planetary waves. The method basically consists of solving the linearized set of equations describing oscillations of a stratified resting atmosphere on a spherical earth by separating the equations into a latitudinal structure equation and vertical structure equation. The vertical structure equation determines the vertical modes of oscillation. The separation constants(eigenvalues) from the vertical structure equation can be used to find the eigenfunctions of the latitudinal structure equation. The latitudinal structure equation for a given eigenvalue is identical to a fundamental equation of a free surface, if the eigenvalue is replaced by the uniform depth of the fluid. This equation was first obtained by Laplace in his study of free oscillations of shallow water over a rotating sphere. For this reason the horizontal structure equation is often referred to as Laplace's tidal equation and the eigenvalues are referred to as equivalent depths. The mode associated with the largest equivalent depth is referred to as the external or barotropic mode. This is because this mode has a vertical profile of horizontal divergence with the same sign throughout the atmosphere. The other modes associated with smaller equivalent depths are referred to as internal modes. These modes are oscillatory in the vertical. For a given equivalent depth, zonal wavenumber and meridional mode there exist three sets of eigenfrequencies and eigenfunctions. Two are eastward-

and westward-propagating gravity waves and the third is a westward propagating Rossby-Haurwitz type wave. The phase speeds of these waves are related to equivalent depth, meridional mode and zonal wavenumber. For the Rossby type wave the fastest phase s peed occurs with the largest equivalent depth and smallest meridional mode and zonal wavenumber. The period of this gravest, symmetric zonal wavenumber one Rossby mode is almost exactly 5 days. There is observational evidence for the existence of this wave (Madden and Julian, 1972) and there is also evidence that some of the planetary wave error in numerical models is in part due to the spurious excitation of these large scale external Rossby modes (Daley et al, 1981). The following transient modes which were observed in the three different parts of this study are:

1. the mode which moved at the speed of the mean wind in the case where the model atmosphere was being brought to a steady state,
2. the mode which moved at the speed of the mean wind in the case where the model heating was turned off,
3. the westward moving modes in the case where error was introduced into the rotational part of the wind.

These modes may be explainable in terms of these external and internal Rossby modes. The mode which is moving at the speed of mean wind may be a slow westward moving internal mode which is overwhelmed by the mean wind. The westward moving modes in the last experiment are most likely internal modes as well but are probably associated with larger equivalent depths than those of the earlier experiments. Since phase speed for a given wavenumber and meridional mode increases with increasing equivalent depth, these waves would have a greater westward phase speed and would be less counterbalanced by the mean wind. Given a large enough westward phase speed one would actually see a westward

propagation indicated on the harmonic dials. The low frequency modes in the first two parts of this study were most likely excited by the discontinuous nature of the forcing. Numerical studies by Geisler and Dickinson (1976) indicate that even when the forcing is gradually turned on that low frequency Rossby modes are excited. An analytic study by Clark (1972) also showed that a mode which moved at the speed of the mean wind would be excited by a switch on of a vertical velocity or temperature disturbance. However, this mode was only one of a number of modes which would be excited and it was also found to decay with time. Thus, it is possible that the transient modes which were observed to move at the speed of the mean wind are in fact internal Rossby modes. The fact that internal Rossby modes might have been excited when errors were introduced into the rotational part of the wind is consistent with the results of Daley et al (1981) who found that errors in the rotational wind will cause a spurious excitation of these modes. However, it must be pointed out that since the results of this study were analyzed using spherical harmonics rather than normal modes it is impossible to confirm the above hypothesis. The question that might now be asked is why wasn't the external barotropic mode excited in these experiments? The studies by Geisler and Dickinson and Clark found that this mode would be excited. Clark found that this mode would in fact be the dominate mode. The crucial difference between the analytic model of Clark , the numerical model of Geisler and Dickinson and the model in this study is that this model does not have a vertical wind shear while the aforementioned models do. This lack of vertical shear is the most probable reason why the barotropic mode was not excited. In the absence of a mean vertical shear the heating specified in this model will produce low pressure at the surface and a high pressure aloft. The vorticities

associated with each will be of the same magnitude so that the vertically averaged vorticity vanishes and there can be no barotropic mode response. When a mean vertical shear is present there is a differential advection affect and the upper and lower vorticities dc not exactly cancel, thus allowing the possiblity of a barotropic mode

Given the slow phase speed of the transient modes excited in this study by 'errors' in the forcing and initial conditions it does not appear that planetary waves are very sensitive to errors. However, this apparent lack of sensitivity is most likely due to the simplified conditions used in the model rather than to the inherent nature of planetary waves. Specifically, the lack of wind shear prohibits the excitation of the fast external Rossby wave. The external mode has a fast phase speed (72 °/day) and if excited it could rapidly propagate throughout the region of integration.

The results obtained by heating in this study might also have been obtained by including topography along with a stronger surface friction term. Future studies should investigate the sensitivity of planetary wave to errors in topography as well as heating. In addition, future studies will have to use a more realistic vertical wind profile. Due to the lack of a realistic wind profile, which prohibits the excitations of the external barotropic mode, any conclusions about the sensitivity of planetary waves to initial conditions and forcing must be delayed until more comprehensive studies are completed.

LIST OF REFERENCES

Arakawa, A., and M. J. Suarez, 1983: Vertical differencing of the primitive equations in sigma coordinates. Mon. Wea. Rev., 111, 34-45.

Baumhefner, D., and P. Downey, 1978: A comparison of six wintertime forecasts from several numerical weather prediction models. Proc. 12th Stanstead Seminar, McGill University Publications in Meteorology No. 121, 98pp. (Department of Meteorology McGill University, 805 Sherbrooke St. W., Montreal P.Q., H3A 2K6 Canada.)

Bourke, W., 1974: A multi-level spectral model 1. Formulation and hemispheric integrations. Mon. Wea. Rev., 102, 687-701.

Clark, J. H. E., 1972: The vertical progagation of forced atmospheric planetary waves. J. Atmos. Sci., 29, 1430-1451.

Daley, R., J. Tribbia, and D. Williamson, 1981: The excitation of large-scale free Rossby waves in numerical weather prediction. Mon. Wea. Rev., 109, 1836-1861.

Geisler, J. E. and R. E. Dicksison, 1976: The five-day wave on a sphere with realistic zonal winds. J. Atmos. Sci., 33, 632-641.

Haltiner, G. J. and R. T. Williams, 1980: Numerical Prediction and Dynamic Meteorology. John Wiley & Sons, 477pp.

Hoskins, B. J. and A. J. Simmons, 1975: A multi-layer spectral model and the semi-implicit method. Quart. J. Roy. Meteor. Soc., 101, 637-655.

Kasahara, A., 1976: Normal modes of ultralong waves in the atmosphere. Mon. Wea. Rev., 104, 669-690.

Lambert, S., and P. Merilees, 1978: A study of planetary wave errors in a spectral numerical weather prediction model. Atmos. Ocean, 16, 197-211.

Lorenz, E., 1969: The predictability of a flow which possesses many scales of motion. Tellus, 21, 248-307.

Madden, R. A. and P. A. Julian, 1972: Further evidence of global-scale 5-day pressure waves. J. Atmos. Sci., 29, 1464-1469.

Morse, P. J., 1983: NOGAPS verification using spectral components. Masters Thesis, Naval Postgraduate School, 71pp.

Rosmond, T. E., 1977: Personal correspondence.

INITIAL DISTRIBUTION LIST

		No. Copies
1.	Defense Technical Information Center Cameron Station Alexandria, VA 22314	2
2.	Library, Code 0142 Naval Postgraduate School Monterey, CA 93943	2
3.	Commander Naval Oceanography Command NSTL Station Bay St Louis, MS 39522	1
3.	Commander Air Weather Service Scott Air Force Base, IL 62225	1
4.	Commanding Officer Fleet Numerical Oceanography Center Monterey, CA 93943	1
5.	Commanding Officer Air Force Global Weather Central Offutt Air Force Base, NE 68113	1
6.	Officer-in-Charge Naval Environmental Prediction Research Facility Monterey, CA 93943	1
7.	Prof. C. N. K. Mooers, Code 63Mr Naval Postgraduate School Monterey, CA 93943	1
8.	Prof. R. J. Renard, Code 63Rd Naval Postgraduate School Monterey, CA 93943	1
9.	Major Patrick Herod AFIT/CIRF Wright-Patterson AFB, OH 45433	2
10.	Air Weather Service Technical Library Scott AFB, IL 62225	1
11.	Captain Michael D. McAtee, Code 63 Naval Postgraduate School Monterey, CA 93943	2
12.	Director of Research and Administration Code 012 Naval Postgraduate School Monterey, CA 93943	1
13.	Prof. R. T. Williams, Code 63Wu Naval Postgraduate School Monterey CA 93943	3

14. Prof. M. A. Rennick, Code 63 — 1
Naval Postgraduate School
Monterey CA 93943

15. Dr. T Rosmond — 1
Naval Environmental Prediction Research Facility
Monterey, CA 93943

16. Dr. J. Hovermale — 1
Naval Environmental Prediction Research Facility
Monterey, CA 93943

17. Prof. C. H. Wash, Code 63 — 1
Naval Postgraduate School
Monterey, CA 93943

END

FILMED

7-85

DTIC